1
Introduction

The group III-Nitride compounds such as Gallium Nitride (GaN), Aluminium Gallium Nitride (AlGaN), Aluminium Nitride (AlN), and Indium Nitride (InN) have made a significant space in the micro and nano-electronic fields. This material family and its compounds have a much broader spectrum of bandgap compared to other semiconductors. Thus, the interest in group III-nitride semiconductors has been developed of the various research groups for the last three decades for optoelectronic, chemical and biosensing, high-power, high frequency, and high-temperature application.

The GaN has covered a long journey to become a crucial material for widespread applications. It was initially reported in 1938 by Juza and Hahn [V. P. Sirkeli *et al.*, 2020], where the synthesis of GaN was carried out by applying ammonia (NH_3) over hot gallium (Ga). After ten years, the growth of GaN was demonstrated using the chemical vapor deposition (CVD) technique for the first time by Maruska and Tietjen [Maruska and Tietjen, 1969]. Further, new technologies were involved in 1960-70 for the development of GaN by utilizing Ga_2O_3 and NH_3 reaction [Lorenz and Binkowski, 1962] and Ga evaporation in nitrogen (N_2) plasma [Kosicki and Kahng, 1969]. In 1971-72, the first GaN-based violet light-emitting diode was proposed by utilizing Mg-doped GaN diodes [Maruska *et al.*, 1972]. Also, the concept of high electron mobility transistor (HEMT) on GaAs was expressed for the first time by T. Mimura et al.[Mimura *et al.*, 1979]. Though, such experiments did not succeed much because of underlying problems in the GaN material properties as there was no bulk-crystal technology for the production of GaN as a substrate. Also, the epitaxial growth of GaN on highly lattice-mismatched substrates results in high defect density and poor surface morphology. Furthermore, the high n-type background doping, in addition to the deep ionization levels of different acceptors, caused the failure in p-type growth of III-nitrides and hence did not use for device fabrication till the late 80s. After 1983, molecular beam epitaxy (MBE) [Yoshida *et al.*, 1983] and metal-organic chemical vapor deposition (MOCVD) [Khan *et al.*, 1983] provided a new dimension for the possible growth of GaN by the improvement of structural and electrical characteristics. Amano and Akasaki [Amano *et al.*, 1990] reported an efficient p-doping using low energy electron beam irradiation of GaN and Mg. This process was further extended by Nakamura in 1992 by thermal annealing at 750°C in the N_2 environment for the fabrication of Mg-doped GaN as p-type material [Nakamura *et al.*, 1992]. Later, in 1993, Khan *et al.* exhibited the AlGaN/GaN high electron mobility transistor for the first time [Khan *et al.*, 1993]. In 1993, Nakamura et al. also achieved blue LED production by utilizing an InGaN/AlGaN heterostructure for which they have awarded the Nobel prize in 2011[Nakamura, 1995; Nakamura *et al.*, 1993]. The advancement of blue LEDs opens the door for the development of the research interest towards blue lasers. Hereafter, in 1995, Nakamura *et al.* fabricated the first-ever III-N based laser diode with continuous-wave emission of 417 nm wavelength at room-temperature [Nakamura *et al.*, 1996]. These discoveries extend the GaN research towards the commercialization of optoelectronic devices. In addition, exceptional electrical and structural properties of GaN boost its utility for high temperature, high power, and high-frequency applications. Moreover, at the beginning of 2000, the AlGaN/GaN heterostructures have been used for mechanical, medical, and sensing applications [Kang *et al.*, 2005; Mehandru *et al.*, 2004].

The AlGaN/GaN heterostructure is an ideal heterostructure for sensing application due to its robustness at high temperature, high physical and chemical stability, excellent biological compatibility, and highly sensitive surface due to availability of surface charges. In addition to these properties, the polar behavior of the III-N semiconductors makes it more advantageous over other materials such as Silicon carbide (SiC), Silicon (Si), and Gallium Arsenide (GaAs). The polarization in AlGaN and GaN results in the formation of charged interfaces that leads accumulation of electrons and holes near the interface and result in very high electron density at AlGaN/GaN heterojunction called two-dimensional electron gas (2DEG). The formation of 2DEG does not require any doping; thus, the absence of doping reduces impurity scattering, and hence electron mobility increases. The high density and high mobility of electrons at 2DEG in AlGaN/ GaN HEMTs provide higher output current density and make the device normally-on, i.e., 2DEG channel formed without application of gate potential. Hence, the AlGaN/ GaN heterostructure is an exceptional candidate for chemical and biosensing, as well as power applications. The AlGaN/GaN high electron mobility transistors (HEMTs) are the devices, can be utilized as sensors by further functionalization of different chemicals to detect target analytes. These can also provide possible monolithic integration with III-Nitride industries to make on-chip and portable sensors for real-time monitoring of analytes.

Due to lake of availability and very high cost of GaN substrates, the fabrication of AlGaN/GaN HEMT is carried out on foreign substrates such as Si, Sapphire, and SiC. In general, sapphire and Si are used as a substrate due to low cost compared to SiC and integration possibility with well-established Si industries. However, these materials have some drawbacks of low thermal conductivity and high lattice mismatch between GaN and Si. The low thermal conductivity results in heat-trapping on the surface of GaN and decreases channel conductivity. When AlGaN/GaN HEMT is used in high power applications, effects such as the self-heating phenomenon degrade the electrical performance of the device. Thus, it is essential to analyze the self-heating behavior of HEMT. The device simulation of AlGaN/GaN HEMT assists in analyzing this effect by revealing a quantitative relationship between the material properties of III-Nitride semiconductors and HEMT behavior. It can be accomplished through the Sentaurus technology computer-aided design (TCAD) simulator tool, where the device simulation was carried out by charge transport equations.

In this chapter, the electrical, material, and physical properties of III-Nitrides are presented. Also, it provides an overview of the AlGaN/GaN high electron mobility transistor. This chapter further describes heavy metal ion sensors, their types, and desirable parameters such as sensitivity, selectivity, response time, and detection limit. Later the literature review for the application of AlGaN/GaN HEMT as a heavy metal ion sensor with motivation towards the work, research objective, and details about the thesis organization is conferred.

1.1 PROPERTIES OF III-NITRIDE MATERIALS

1.1.1 Crystal Structure

The group III-Nitride materials (AlN, GaN, InN) generally found in wurtzite hexagonally close-packed (HCP) and zincblende crystal structures. At room temperature, the wurtzite crystal structure is a thermodynamically stable form of III-Nitrides; thus, the wurtzite crystal structure is more preferred for the fabrication of the III-Nitride devices such as HEMT. The wurtzite structures of III-N, such as GaN, are tetrahedrally coordinated, having four atoms per unit cell in a Bravais lattice structure, as shown in Figure 1.1. There are three lattice constants, which entirely define wurtzite structure, the length of the hexagonal base side called a height of the cell c, and a dimensionless parameter u defined as the bond length of cations and anions. This dimensionless parameter describes the GaN bonds in the multiple of c. The ratio of these lattice parameters for an ideal wurtzite structure is $c/a = \sqrt{8/3} \approx 1.633$ and u = 3/8 = 0.375 [Morkoc, 2008]. The lattice parameters of III-Ns have been described in Table 1.1.

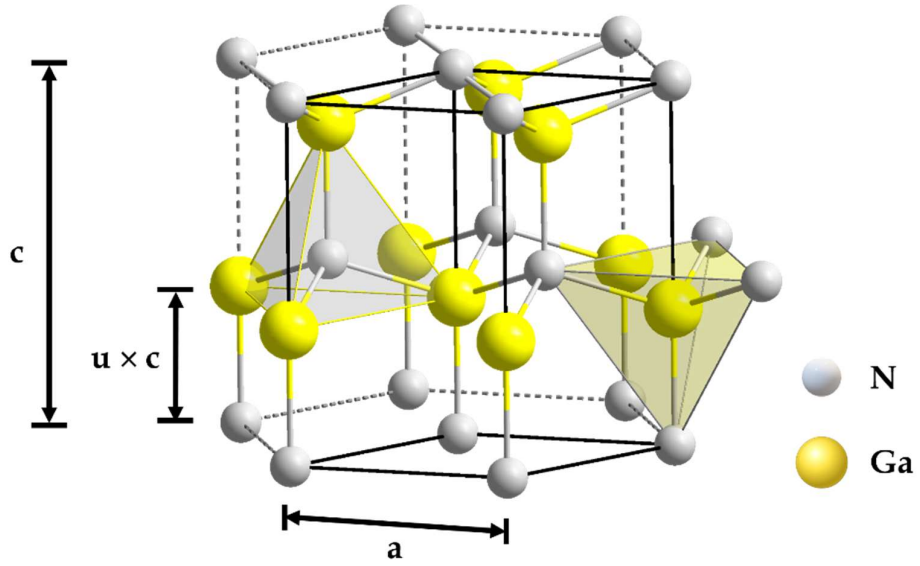

Figure 1.1: Wurtzite hcp structure of GaN comprising tetrahedral coordination of Ga and N atoms with lattice constant a and c (source: reproduced from [Kente and Mhlanga, 2016] by permission of the Elsevier).

In the wurtzite structure of III-nitrides, each sublattice consists of either Nitrogen or group III element(s) forming anions and cations, respectively. Herein, each Nitrogen atom coordinated with four group III atoms and vice versa. The growth of III-N materials is usually performed along the c-axis in the wurtzite crystal structure. III-Nitride materials such as GaN possess non-centrosymmetric crystal structure along the c axis, which means the crystal has a different sequence of atoms when one atom moves from one side of the crystal to the other side. Thus, the Ga and N atoms assemble themselves in atomic bilayers, resulting in polar faces because of the higher electronegativity difference between Ga and N atoms [Ambacher *et al.*, 1999b] and can be grown in the Ga-face or N-face. Figure 1.2 shows a stick and ball model of Ga polarity and N polarity of GaN wurtzite structure. In general, the convention [0 0 0 1] shows the direction of the crystal along the c-axis from N face to Ga face in GaN, and the polarity is called Ga polarity, which indicates +z direction. Similarly, when the bonds between Ga and N are from N to Ga atoms along the c-axis, the polarity is given as the N-polarity, which is generally indicated as -z-direction [Morkoc, 2008].

Table 1.1: lattice parameters of III-N semiconductors for wurtzite structure [Morkoc, 2008]

Parameter	*GaN*	*AlN*
a (Å)	3.189	3.1106
c (Å)	5.1864	4.9795

The development of Ga-face and N-face structures relies on the different growth conditions. Both of these polarities have distinct properties that can affect device technology as well as the performance of the device. The N-face structures have a chemically active surface, which allows wet-chemical etching of the material; however, they experience a very rough surface morphology and can suffer high background doping concentration. Whereas, the Ga-face structures have very smooth surface morphology and low background doping concentration compared to N-face, which is helpful for improved device performance. The Ga-face material structures are almost chemically inert and can only be etched using a plasma etching technique. Because of these superior material properties, Ga-face structures are preferred for device applications.

1.1.2 Polarization in III-N Semiconductors

In III-N semiconductors, polarization is a fundamental property that defines the actual operation of the III-N devices such as HEMTs. Polarization is a macroscopic property of materials where the dissimilarity in electronegativity of the atoms create bonds with each other. This effect causes the displacement of cation and anion charge centers that crates the dipoles with dipole moments. The term polarization (P) can be defined merely as the dipole moment per unit volume. Polarization of the material highly depends on the crystal polarity, i.e., the direction of the c-axis has the atomic bonds towards group-III material side or N-side. The group III-nitrides comprise two types of polarization. These are:

(a) Spontaneous polarization.

(b) Piezoelectric polarization.

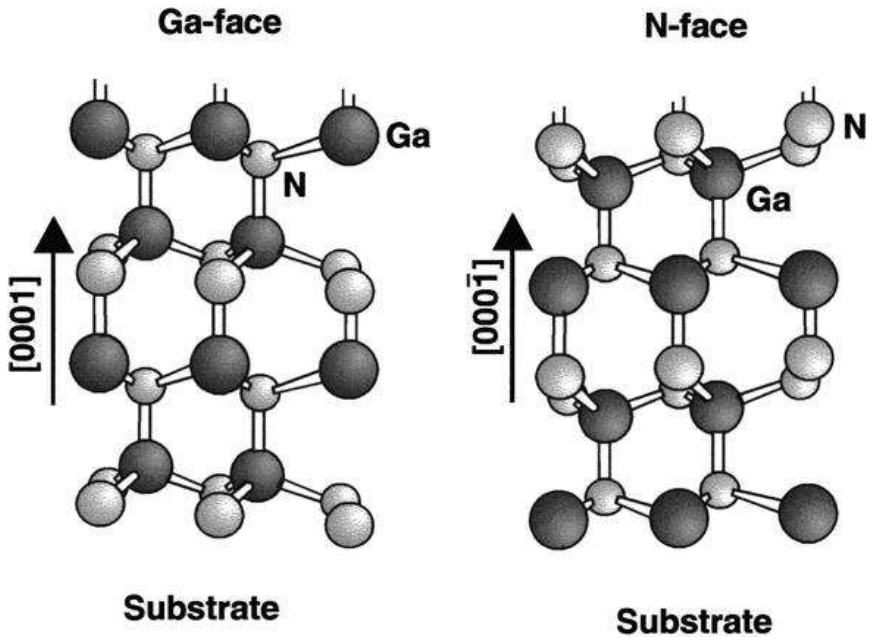

Figure 1.2: Stick and ball representation of Ga face and N face wurtzite crystal structure (source: reproduced from [Ambacher *et al.*, 1999b] by permission of the AIP Publishing).

(a) Spontaneous Polarization

Spontaneous polarization is an inherent property of the solid that relates to the bond nature of the material. The spontaneous polarization can be defined as it is the polarization at zero strain. The spontaneous polarization cannot change by the applied electric field or any other applied external force. This property is a bulk effect because of the higher electronegativity of nitrogen that defines the ionic character of group-III nitrides. As discussed in the previous sub-section, the materials with wurtzite crystal structure such as GaN, AlN, and other III-Ns possess non-centrosymmetric structure along the c-axis. This lack of inversion symmetry in the III-nitride semiconductors makes the presence of an inherent electric field in the material. This electric field can cause the formation of a permanent dipole moment in the semiconductor, which results in spontaneous polarization (P_{SP}) [Bernardini, 2007]. The polarity of the wurtzite crystal of the III-N semiconductors determines the sign of spontaneous polarization. This sign is contrary to the [0001] direction, as shown in Figure 1.3. Further, the spontaneous polarization nonlinearly depends on the mole fraction of Al in AlGaN. The values of polarization for different binary nitride elements such as AlN and GaN have been shown in Table 1.2. It can be seen from the table that AlN has significantly stronger spontaneous polarization than GaN and has a negative sign, which indicates that the Ga-face materials have spontaneous polarization pointing from surface to bulk.

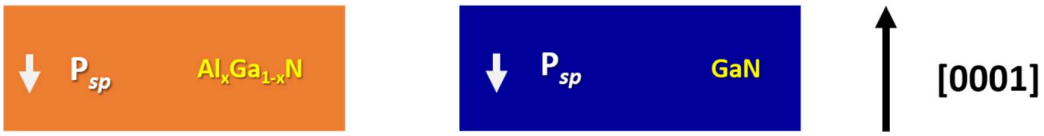

Figure 1.3: Spontaneous polarization in GaN and AlGaN materials, grown in [0001] direction.

(b) Piezoelectric Polarization

Piezoelectric polarization is the polarization that induces in a material by the mechanical strain. There are two types of piezoelectric polarization, the direct piezoelectric polarization, in which the applied strain to the material generates the potential, and the converse piezoelectric polarization, where an applied potential produces mechanical strain to the material. Generally, the piezoelectric materials show time-varying dipole moments by an applied time-varying mechanical strain. Two factors can cause the piezoelectric polarization, in which one is thermal strain caused by thermal expansion coefficient mismatch between epilayers and the substrate, and another one is lattice mismatch strain. In general, the wurtzite structures show excellent piezoelectric polarization behavior, and the group III-nitrides no exception. The III-N materials show direct as well as converse piezoelectric polarization behavior. These materials demonstrate superior piezoelectric polarization than other III-V semiconducting materials.

The piezoelectric polarization in III-N semiconductors was derived by [Ambacher *et al.*, 2002], utilizing Hooke's law. The deformation of a crystal ε_{kl} owing to internal or external forces or strain and stresses σ_{ij}, can be described by this law as:

$$\sigma_{ij} = \sum_{k,l} C_{ijkl}\varepsilon_{kl} \tag{1.1}$$

where C_{ijkl} is the fourth-rank elastic tensor, which can be reduced to 6 × 6 matrices due to spatial symmetry of wurtzite crystal structure. The elements of the elastic tensor can be rewritten as:

$$C_{ijkl} = C_{mn} \tag{1.2}$$

where $m, n = 1, \ldots, 6$. By considering $i, j, k, l = x, y, z$ and utilizing Voigt notation $xx \rightarrow 1$, $yy \rightarrow 2$, $zz \rightarrow 3$, $yz, zy \rightarrow 4$, $zx, xz \rightarrow 5$, $xy, yx \rightarrow 6$, Hooke's law can be rewritten as:

$$\sigma_{ij} = \sum_{j} C_{ij}\varepsilon_{j} \tag{1.3}$$

The elastic constant C_{ij} with 6 × 6 matrices for wurtzite crystal structure can be given as:

$$C_{ij} = \begin{pmatrix} C_{11} & C_{12} & C_{13} & 0 & 0 & 0 \\ C_{12} & C_{11} & C_{13} & 0 & 0 & 0 \\ C_{13} & C_{13} & C_{33} & 0 & 0 & 0 \\ 0 & 0 & 0 & C_{44} & 0 & 0 \\ 0 & 0 & 0 & 0 & C_{44} & 0 \\ 0 & 0 & 0 & 0 & 0 & \frac{1}{2}(C_{11} - C_{12}) \end{pmatrix} \tag{1.4}$$

It was observed that the binary compounds with wurtzite crystal structure have isotropic hardness in the basal plane [Ambacher *et al.*, 2002]. It is an important fact as the epitaxial layers of III-N heterostructures grown along with the [0001] axis or *c*-axis experience strain due to lattice mismatch of the lattice constants *a* and the difference between the thermal expansion coefficients of III-N layers and substrate. Since there is no force applied in the growth direction (c-axis) and the crystal is freely relaxed along [0001] axis; thus, the resulting biaxial strain, $\varepsilon_1 = \varepsilon_2$ generates

stress $\sigma_1 = \sigma_2$, while stress σ_3 is zero. Hence, the relation between the strain along with the [0001] axis of the wurtzite crystal structure and the basal plane can be obtained by utilizing the Eq. (1.3) and Eq. (1.4) and given as:

$$\varepsilon_3 = -2\frac{C_{13}}{C_{33}}\varepsilon_1 \tag{1.5}$$

where ε_1 and ε_3 are the relative changes to the lattice constants a and c with respect to the relaxed crystals a_0 and c_0 respectively can be given as:

$$\varepsilon_1 = \frac{a - a_0}{a_0} \quad \text{and} \quad \varepsilon_3 = \frac{c - c_0}{c_0} \tag{1.6}$$

Due to the lattice mismatch, the stress in the basal plane caused and can be calculated as:

$$\sigma_1 = \varepsilon_1\left(C_{11} + C_{12} - 2\frac{C_{13}^2}{C_{33}}\right) \tag{1.7}$$

where

$$C_{11} + C_{12} - 2\frac{C_{13}^2}{C_{33}} > 0$$

In hexagonal crystal structures, the piezoelectric polarization is associated with strain by the piezoelectric tensor ($e_{i,j}$), can be given as:

$$P_i^{pz} = \sum_j e_{ij}\varepsilon_j \tag{1.8}$$

where i= 1, 2, 3 and j= 1, 2, …., 6; and P_i^{pz} , and ε_j represents the piezoelectric polarization of i^{th} component and strain, respectively. Piezoelectric polarization can also be expressed in terms of piezoelectric moduli d_{ij} as:

$$e_{ij} = \sum_k d_{ik}C_{kj} \tag{1.9}$$

where i = 1, 2, 3; j and k = 1, 2, …., 6. By utilizing the Eq. (1.8) and Eq. (1.9), the piezoelectric polarization can relate with piezoelectric moduli as:

$$P_i^{pz} = \sum_j d_{ij}\sigma_j \tag{1.10}$$

Owing to symmetry relations, $d_{31} = d_{32}$, $d_{15} = d_{24}$, $d_{33} \neq 0$ and remaining all other components $d_{ij} = 0$, and hence the Eq. (1.8) reduces to a set of three different equations:

$$P_1^{pz} = \frac{1}{2}\, d_{15}\sigma_5 \tag{1.11}$$

$$P_2^{pz} = \frac{1}{2}\, d_{15}\sigma_4 \tag{1.12}$$

$$P_3^{pz} = d_{31}(\sigma_1 + \sigma_2) + d_{33}\sigma_3 \tag{1.13}$$

In case of epitaxial layers, for biaxial stress $\sigma_1 = \sigma_2$, $\sigma_3 = 0$. Furthermore, the shear stresses are also negligible, thus $\sigma_4 = \sigma_5 = 0$. Hence, by considering these parameters and Eq. (1.7), there is

only one non-vanishing component in the piezoelectric polarization directed towards the growth direction and is given as:

$$P_3^{pz} = 2d_{31}\sigma_1 = 2d_{31}\varepsilon_1\left(C_{11} + C_{12} - 2\frac{C_{13}^2}{C_{33}}\right) \tag{1.14}$$

The relations between piezoelectric constants and moduli have been described in Eq. (1.9) can be reduced for hexagonal crystals and given as:

$$e_{31} = e_{32} = C_{11}d_{31} + C_{13}d_{33} = (C_{11} + C_{12})d_{31} + C_{13}d_{33} \tag{1.15}$$

$$e_{33} = 2C_{13}d_{31} + C_{33}d_{33} \tag{1.16}$$

$$e_{15} = e_{24} = C_{44}d_{15} \tag{1.17}$$

whereas $e_{ij} = 0$ for all other components. Furthermore, using Eq. (1.8), the non-vanishing component of the piezoelectric polarization owing to the biaxial strain for $i = 3$ can be given as:

$$P_3^{pz} = \varepsilon_1 e_{31} + \varepsilon_2 e_{32} + \varepsilon_3 e_{33} \tag{1.18}$$

By using equations (1.15) and (1.5), the Eq. (1.18) can be rewritten as:

$$P_3^{pz} = 2\varepsilon_1\left(e_{31} - e_{33}\frac{C_{13}}{C_{33}}\right) \tag{1.19}$$

It can be observed from Eq. (1.19) and (1.6) that the piezoelectric polarization towards the growing direction (*c*-axis) linearly depends on the relative change in the lattice constant *a*. Moreover, the piezoelectric polarization is always positive for epitaxial layers under compressive strain and negative for epitaxial layers experiencing biaxial tensile strain, as shown in Figure. 1.4. Due to this fact, the piezoelectric and spontaneous polarization are pointing towards the $[000\bar{1}]$ direction for biaxial tensile strain, whereas under biaxial compressive strain, the orientation of the piezoelectric polarization in the crystal towards the [0001]-axis is the opposite to spontaneous polarization. Table-1.2 shows the values of the ε_{ij}, e_{ij}, and d_{ij} coefficients and corresponding spontaneous polarization for GaN and AlN, as reported in the literature.

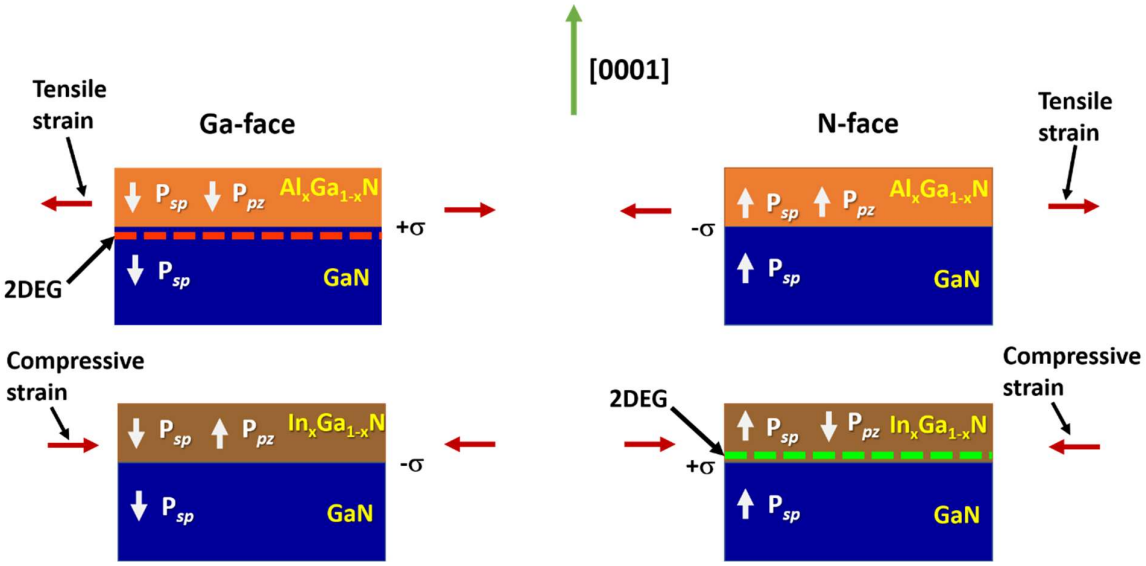

Figure 1.4: Orientation of the piezoelectric and spontaneous polarization in wurtzite AlGaN/GaN and InGaN/GaN heterostructures with Ga- and N-face polarity with tensile and compressive strain [Ambacher *et al.*, 1999b].

Furthermore, the III-nitride heterojunctions and devices such as high electron mobility transistors use ternary alloys such as AlGaN as well. The piezoelectric polarization parameters for binary nitrides are generally sufficient to describe these parameters for more complex alloys such as AlGaN and AlInN. Thus, it becomes straightforward to evaluate the piezoelectric polarization of the $A_xB_{1-x}N$ alloy at any strain for a value of the mole fraction of Al, x in AlGaN [Ambacher *et al.*, 2002]. In the case of $Al_xGa_{1-x}N$, the expression for piezoelectric polarization, using binary nitride parameters, can be described as using Vegard's law:

$$P_{AlGaN}^{pz} = x\, P_{AlN}^{pz}\, \varepsilon(x) + (1-x) P_{GaN}^{pz}\, \varepsilon(x) \tag{1.20}$$

where $P_{AlN}^{pz}\, \varepsilon(x)$ and $P_{GaN}^{pz}\, \varepsilon(x)$ are strain-dependent piezoelectric polarization parameters of AlN and GaN

Table 1.2: Values of different piezoelectric coefficients in wurtzite GaN and AlN, as reported in the literature.

Parameters	*GaN*	*AlN*	*Reference*
e_{31} (C/m^2)	-0.49	-0.60	[Ambacher *et al.*, 1999a]
e_{33} (C/m^2)	0.73	1.46	[Ambacher *et al.*, 1999a]
e_{15} (C/m^2)	0.3	-0.48	[Ambacher *et al.*, 1999a]
C_{11} (GPa)	367	396	[Ambacher *et al.*, 2002]
C_{12} (GPa)	135	137	[Ambacher *et al.*, 2002]
C_{13} (GPa)	103	108	[Ambacher *et al.*, 2002]
C_{33} (GPa)	405	373	[Ambacher *et al.*, 2002]
C_{44} (GPa)	95	116	[Ambacher *et al.*, 2002]
d_{31} (pm V^{-1})	-1.253	-2.298	[Ambacher *et al.*, 2002]
d_{33} (pm V^{-1})	2.291	5.352	[Ambacher *et al.*, 2002]
d_{15} (pm V^{-1})	-1.579	-2.069	[Ambacher *et al.*, 2002]
P^{sp} (C/m^2)	-0.029	-0.081	[Ambacher *et al.*, 1999a]

1.1.3 Bandgap

The binary and ternary compounds of III-N semiconductors such as GaN, InN, AlN $Al_xGa_{1-x}N$, and $In_xGa_{1-x}N$ provide a continuous and extensive range of bandgap values by a small change related to the lattice constant. Figure 1.5 shows the bandgap vs. lattice-constant analysis of semiconductor materials. The bandgap of InN, GaN, and AlN is 0.8 eV, 3.42 eV, and 6.2 eV, respectively [Quay, 2008], provides an incredibly wide range of energies; hence these material group covers the wavelengths ranges from the deep ultraviolet to infrared. Additionally, the bandgap size is a decisive factor for device operation at high temperatures.

The wide range of bandgap of III-N semiconductors paves a way to miniaturize devices that can endure the heat generation during the device operation better than conventional materials of group-IV. These specialties of III-N materials were unchallenged by any other group of materials.

1.2 AlGaN/GaN HETEROSTRUCTURE AND CONCEPT OF 2-DIMENSIONAL ELECTRON GAS (2DEG)

A heterostructure or heterojunction is formed between two different semiconductors grown one over another having the same crystal structure but different energy bandgaps, E_g, work functions $q\phi_s$, and electron affinities χ_s. The difference between the lattice constant of both of the semiconductors describes the quality of the heterostructure. Larger lattice mismatch

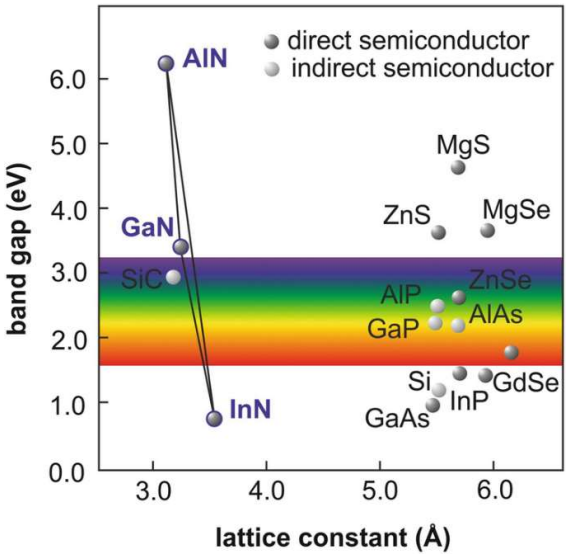

Figure 1.5: Bandgap vs. lattice constants of III-Ns and other semiconductors. (Source: [Cimalla, 2018] reprinted with the permission of the Springer Nature).

increases the possibility of the interfacial defect densities and hence poor quality of heterostructure.

When a heterojunction is formed between two semiconductors having different energy bandgap, causes bandgap discontinuity (ΔE_g) in the structure [Balaz, 2011]. It is also called a total bandgap difference and can be given as:

$$\Delta E_g = \Delta E_C + \Delta E_V \tag{1.21}$$

where ΔE_C and ΔE_V are energy bandgap discontinuity in conduction and valency band, respectively. ΔE_g is an essential parameter for the performance analysis of the devices having heterostructures such as HEMTs [Piprek, 2007]. In continuation of this, the ΔE_C can also be determined as:

$$\Delta E_C = q\,(\chi_1 - \chi_2) \tag{1.22}$$

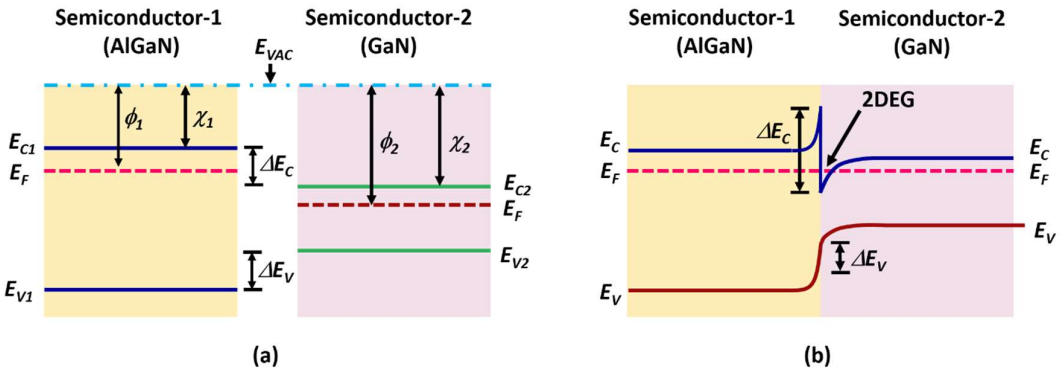

Figure 1.6: Energy band diagram for the narrow (GaN) and wide bandgap (AlGaN) materials with (a) Band offsets before the formation of heterojunction (b) Band bending after heterojunction formation

Figure 1.6 illustrates the energy band diagram of AlGaN and GaN semiconductors before and after the heterojunction formation. While making AlGaN and GaN semiconductors into contact, the band bending occurs at the heterojunction signified by the flat Fermi level. This band bending and discontinuity in the conduction band (ΔE_C) forms a triangular quantum well or a notch in the conduction band and a valley in the valence band at the AlGaN/GaN heterointerface

as shown in Figure 1.6 (b). The relative position of this triangular quantum well with respect to the Fermi level is in the GaN, the narrower bandgap material, and its depth describes the charge carrier density. Hence it defines the formation of two-dimensional electron gas (2DEG) at the heterointerface [Balaz, 2011]. The 2DEG is formed at the heterointerface as the electrons get trapped in the triangular quantum well, allowing their movement in only two dimensions along the heterojunction. In general, the AlGaN/GaN heterostructures with Ga-face are undoped; thus, the sheet carrier concentration $n_s(x)$ for undoped AlGaN/GaN heterostructure with Ga-face can be determined by employing the total polarization induced sheet charge $\sigma(x)$ and can be calculated as [Ambacher *et al.*, 1999b]:

$$n_s\,(x) = \frac{\sigma\,(x)}{q} - \left(\frac{\varepsilon_0 \varepsilon(x)}{d_{AlGaN} q^2}\right)[q\emptyset_b(x) + E_F(x) - \Delta E_C(x)] \tag{1.23}$$

where q is the charge on the electron, ε_0 and ε_r is the permittivity and the relative permittivity of the vacuum and the AlGaN, respectively. The $q\phi_b(x)$ is the Schottky barrier height, d_{AlGaN} is the thickness of the AlGaN barrier layer, and E_F is the Fermi energy level concerning the conduction-band-edge of GaN.

Other wide bandgap III-V semiconductors such as GaAs and AlGaAs and the devices based on these materials like HEMT have the electron separation from their donor atoms and accumulated in the quantum well AlGaAs/GaAs heterointerface to form 2DEG. This electron separation from their donor sites significantly decreases the Coulomb scattering that provides high mobility of the electrons at the 2DEG channel. Contrary to III-V semiconductors where doping is required for the 2DEG formation, the III-N semiconductors need not require any doping to form 2DEG due to their unique polarization property. As mentioned above in section 1.1.2, spontaneous and piezoelectric polarization causes the formation of 2DEG at the heterointerface of AlGaN/GaN. Thus, the unique combination of polarization property of AlGaN and GaN and the formation of quantum well at the AlGaN/GaN heterojunction makes it a superior candidate for device fabrication that can be used in various applications such as high power, high frequency, high temperature, optoelectronic, and various sensing applications, e.g., gas, ion, bio and pressure applications.

Apart from these, while utilizing the semiconductors AlGaN and GaN for the heterojunction formation, the aluminum mole fraction in AlGaN must be considered as it defines and modulates the lattice constant and energy bandgap of AlGaN as shown in Figure 1.5. Furthermore, in the AlGaN/GaN heterostructure, the piezoelectric polarization largely depends upon the Al-mole fraction as well as the thickness of the AlGaN layer. Increment of the Al-content in the AlGaN improves piezoelectric polarization, P_{PZ} in the AlGaN/GaN heterostructure. The direction of spontaneous and piezoelectric polarization and corresponding polarization induced sheet charge density in the Ga-face AlGaN/GaN heterostructure were depicted in Figure 1.4. Using the Gauss law, the relation between polarization induced sheet charge density, σ (C/cm^2) and polarization vectors, P_{SP}, and P_{PZ} in the AlGaN/GaN heterostructure can be given as:

$$\sigma\,(x) = P^{SP}_{AlGaN(x)} + P^{PZ}_{AlGaN(x)} - P^{SP}_{GaN} \tag{1.24}$$

Thus, the overall polarization induced charge density increases by increasing the Al mole fraction in the AlGaN layer, and hence the proper utilization of Al-mole fraction in the AlGaN layer for AlGaN/GaN heterointerface is crucial to achieving the high sheet carrier density with high electron mobility in the formation of high electron mobility transistors.

Moreover, the modification in the AlGaN/GaN heterostructures with thin interfacial layer incorporation of AlN of few nanometers sandwiched between AlGaN and GaN layers reported in different kinds of the literature [Parish *et al.*, 2004; Shen *et al.*, 2001]. This improvement

in the AlGaN/GaN heterostructure expresses higher electron mobility over conventional AlGaN/GaN structures [Wang *et al.*, 2007]. Also, the higher performance of AlGaN/AlN/GaN structure is due to the increment in ΔE_C, which efficiently reduces the electron penetration to the AlGaN layer from the GaN layer and decreases alloy disorder scattering.

1.3 AlGaN/GaN HIGH ELECTRON MOBILITY TRANSISTOR

The device for a wide area of interest, including high power, high frequency, optical, and various sensing applications like bio, gas, and ions, is AlGaN/GaN HEMT. An AlGaN/GaN HEMT is also called a heterojunction field-effect transistor (HFET) and modulation doped field effect transistor (MODFET), which belongs to the family of field-effect transistors (FET). The structure of AlGaN/GaN HEMT provides the attractive characteristics of gate proximity to the 2DEG with high transconductance along with the high low-field mobility, high electron sheet densities, high maximum drift velocity, which makes the AlGaN/GaN HEMT suitable for different applications as described above.

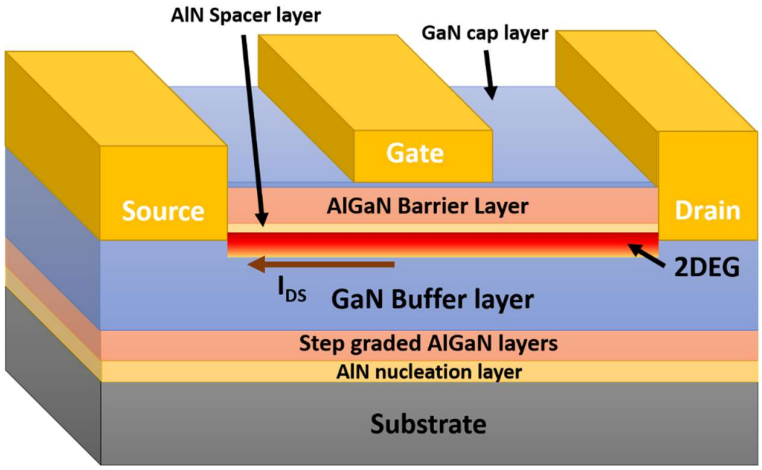

Figure 1.7: Epitaxial structure of AlGaN/GaN HEMT.

1.3.1 Basic Structure of AlGaN/GaN HEMT

The basic structure of AlGaN/GaN HEMT requires an epitaxial growth or a layer by layer structures of several III-N materials for minimizing the defect densities and compensating the lattice mismatch between substrate and GaN, and the improvement of the device performance. Generally, there are two methods used for the epitaxial growth of AlGaN/GaN HEMT, molecular beam epitaxy (MBE) and metal-organic chemical vapor deposition (MOCVD). The device structure of AlGaN/GaN HEMT used in this Thesis, as well as the most commonly used epitaxial structure, is shown in Figure 1.7. Usually, the typical growth of epitaxy for AlGaN/GaN HEMT structure contains the following layers (bottom to top) [Quay, 2008]:

(1) *Substrate:* Due to the lack of availability and very high cost, the growth of AlGaN/GaN HEMTs is challenging on GaN substrates [Gurnett and Adams, 2006]. Alternatively, the substrates of other materials like sapphire (Al_2O_3), Silicon Carbide (SiC), and Silicon (Si) are typically used for the fabrication of AlGaN/GaN HEMT in the literature for different studies and applications [Bajaj *et al.*, 2015; Chen *et al.*, 2008; Nigam *et al.*, 2017]. The details related to substrate choice would be explained in subsection 1.3.2.

(2) *Nucleation layer:* The Nucleation layer is essential because of the high lattice mismatch between the substrate materials and GaN, which results in a low-quality epi layer with high surface roughness. This layer diminishes the threading dislocation densities in the GaN buffer layer. In order to develop high-quality AlGaN/GaN HEMTs, the buffer layer of GaN

should be highly resistive, and the nucleation layer plays a crucial role in it. It is fabricated between the substrate and GaN buffer layers, as shown in Figure 1.7. Different materials such as AlN and AlGaN layers were utilized for the nucleation layer for different substrate materials with different growth temperature and thickness.

(3) *Step graded AlGaN layers:* In addition to the AlN nucleation layer, step-graded AlGaN can be utilized on Si substrates. These step graded AlGaN layers have continuous decrement of Al-mole fraction from the AlN nucleation layer to the GaN buffer layer, which in turn provides smoother transitions between the substrate to GaN of different lattice constants as compared to a single nucleation layer. This addition of step-graded layers enhances the quality of the GaN buffer layer by reducing dislocation densities.

(4) *GaN buffer layer:* In order to achieve the high performance of the device, the quality of the GaN buffer layer should be very high. It means the buffer layer should have low defect density and high resistivity to prevent charge trapping of 2DEG and buffer leakage problems. The thickness of the buffer layer also has significant importance. The thickness of the buffer layer varies between 350 nm to 5 µm as observed from the literature [Ao *et al.*, 2003; Micovic *et al.*, 2001; Quay, 2008]. The thin buffer layer has the advantage of providing less growth time and reduced thermal impedance, whereas the thicker buffer layer minimizes threading dislocation densities and impact due to the residual strain as of the lattice-mismatch. The thicker buffer layer provides a smoother surface with lowered dislocation density and better interface roughness. The only disadvantage of a thicker buffer layer has the thermal impedance to the substrate [Quay, 2008].

(5) *Spacer layer:* As the development of the AlGaN/GaN HEMT was carried out, there is an improvement in the form of a thin space layer at the AlGaN/GaN heterointerface was made. A space layer is a very thin layer (1-2 nm) sandwiched between the AlGaN barrier layer and the GaN buffer layer. It considerably reduces the alloy scattering between the ionized atoms in the barrier layer and corresponding electrons in 2DEG, which extensively improved the mobility of electrons in 2DEG. The spacer layer also improves electron density in 2DEG by providing a high polarization field between GaN and AlN. The other advantages of the utilization of the AlN spacer layer were also discussed in section 1.2.

(6) *Barrier layer:* In the structure of AlGaN/GaN HEMT, this layer is one of the most crucial layers. The barrier layer is made by the AlGaN, which has a wider bandgap than the GaN buffer layer, which helps to form a quantum well at the heterointerface of AlGaN/GaN. The thickness and Al content in the AlGaN barrier layer also plays an important role in the performance of AlGaN/GaN HEMT. Hence, the relation between the thickness of the barrier layer and the impact of the Al mole fraction on AlGaN/GaN heterointerface was discussed in detail in section 1.2.

(7) *Cap layer:* In the epitaxial growth of the AlGaN/GaN structure, the cap layer is the topmost layer (except the passivation layer). It is a thin layer of GaN (1-2 nm), which is deposited over the AlGaN barrier layer to avoid the oxidation of the surface. Another advantage of using the GaN cap layer is to improve the Schottky barrier height and hence reduce the gate leakage current. The enhancement in the Schottky barrier height also improves the flat band voltage [Acar, 2009].

1.3.2 Substrates for AlGaN/ GaN HEMTs

As explained above, the lack of availability and expensiveness of the GaN substrates, the AlGaN/GaN HEMTs, are grown on the substrates of foreign materials. In order to grow the AlGaN/GaN HEMTs on other substrates, specific criteria need to be considered for the choice of substrate. These are:

(1) Lattice mismatch of the substrates related to the epilayers of the HEMTs.

(2) Thermal expansion coefficient the substrate
(3) Thermal conductivity of the substrate material
(4) Cost and price per unit area
(5) Availability of the substrates in terms of diameter

Table 1.3 summarizes the basic properties of the different substrate materials required for the substrate choice for the AlGaN/GaN HEMT structure. In general, there are three types of materials utilized as a substrate for the development of AlGaN/GaN HEMT. These are sapphire (Al_2O_3), silicon carbide (SiC), and Silicon (Si). The details description for these materials towards the development of AlGaN/GaN HEMT is explained below:

(a) Sapphire (Al_2O_3) Substrate

Initially, the single-crystal sapphire is frequently used for the development of AlGaN/GaN heterostructures. Sapphire is an exciting option due to its semi-insulating behavior and capability to sustain at high growth temperatures. Also, it is comparatively very cost-effective and readily available in a 2-4-inch diameter size. Though, large lattice (16%) and thermal expansion coefficient mismatch of 16% and 34% respectively, and very low thermal conductivity of sapphire 50 $W.m^{-1}.K^{-1}$, with respect to the epitaxial layer of GaN make it less suitable for high-power applications [Quay, 2008]. Further, the large lattice mismatch induces stress and wafer bowing, which creates several processing issues.

(b) SiC Substrate

SiC is the fascinating material for substrate choice for AlGaN/GaN HEMT fabrication because of the unique combination of properties such as low lattice mismatch (3.4%), high thermal conductivity 370 $W.m^{-1}.K^{-1}$, and excellent thermal expansion coefficient. The SiC substrates are available with these exceptional properties up to 4-inch diameter size. The excellent surface properties of the GaN are observed for 2DEG on the SiC substrate. Despite all these advantages, the very high cost of SiC limits the fabrication of the AlGaN/GaN HEMT for commercial purposes.

(c) Si Substrate

As Si is dominating materials for the last six decades, the quality and economical use of the Si makes it the most important candidate for substrate choice. However, the Si substrates have a large lattice mismatch (17%) and low thermal expansion coefficient (3.59×10^{-6} K^{-1}) but the low cost, moderate thermal conductivity around 150 $W.m^{-1}.K^{-1}$ at RT, ease of availably in large diameters (8-inch) make them an exciting candidate for the development AlGaN/GaN HEMT devices. Besides this, in terms of the defects, the substrate quality of Silicon is exceptional than SiC and sapphire [Quay, 2008]. Si substrates are available almost defect-free, which improves the reliability of the device. In order to overcome the issues related to the silicon substrates, the epitaxial growth of the different layers is performed, as described in subsection 1.3.1. By using the epitaxial layer growth, the AlGaN/GaN HEMTs were fabricated on silicon (111) substrates with a 200 mm diameter [Tripathy *et al.*, 2012]. Since the growth of AlGaN/GaN HEMTs has been done on the hexagonal phase on the Si (111) plane, hence, an effective lattice constant of Si (3.84 Å) can be utilized and has been shown in Table-1.3[Quay, 2008].

Table 1.3: Properties of substrate materials for AlGaN/GaN HEMT substrate choice [Quay, 2008]

Material	Lattice constant a(Å)	Lattice mismatch to GaN (%)	Thermal expansion coefficient (10^{-6} K^{-1})	Thermal conductivity ($W.m^{-1}K^{-1}$)
GaN	3.189	0	5.59	130
SiC	3.08	3.4	4.2	370
Sapphire	2.747	13	7.5	50
Silicon (111)	3.84	17	3.59	150

1.3.3 Working Principle of AlGaN/GaN HEMT

A generalized schematic demonstration of the AlGaN/GaN HEMT device structure is shown in Figure 1.8. An AlGaN/GaN HEMT is a three-terminal device having Source (S), Drain (D), and Gate (G) terminals. The working principle HEMT is analogous to a Field Effect Transistor, where the current between drain and source terminals is controlled by the electrical field produced by the applied voltage at the gate terminal. The current flows between the drain and source through the 2DEG work as conducting channel similarly to FET, and gate controls the flow of electron in the 2DEG. The quality of this channel or 2DEG depends on the substrate choice and growth process of AlGaN/GaN HEMT. The conductivity of the 2DEG channel is determined by [Sze and Lee, 2012]:

$$\sigma = qn_s\mu \tag{1.25}$$

where q is the charge on electrons, ns sheet carrier concentration of electrons, and μ is the electron mobility at 2DEG. The above equation suggests that the conductivity of the channel is the function of sheet carrier concentration and electron mobility at 2DEG; these two are the important parameters for analysis of HEMT performance. Figure 1.7 shows the layer by layer structure of AlGaN/GaN HEMT along with 2DEG. In the HEMT, the contact to 2DEG is made by thermal annealing of the deposited metals, as discussed in upcoming chapters.

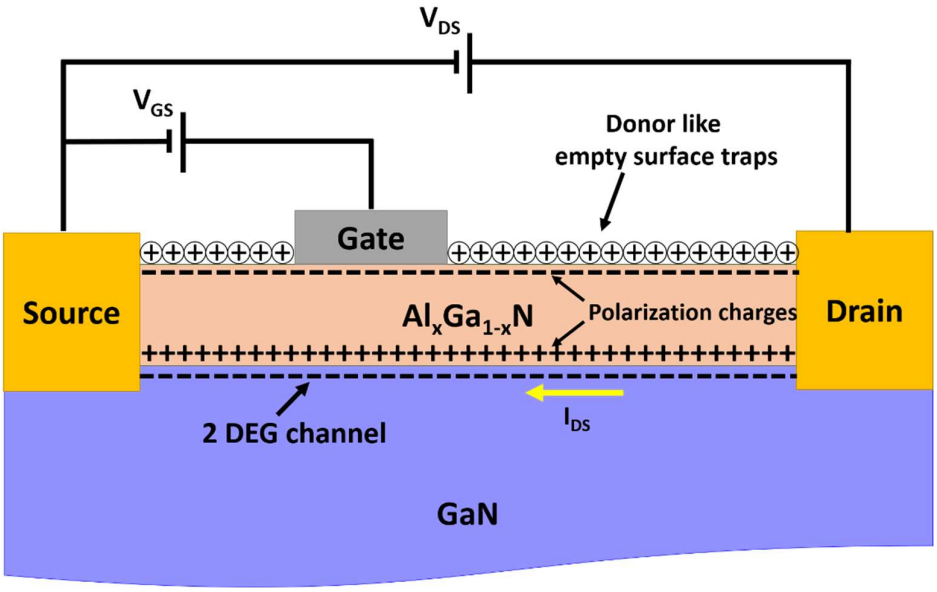

Figure 1.8: Device schematic of AlGaN/GaN HEMT

As explained previously, due to the spontaneous and piezoelectric polarization properties of AlGaN and GaN and the quantum well formation at the AlGaN/GaN heterojunction, the 2DEG is formed at the heterointerface without applying any external field. Thus, the HEMT has an extensive flow of drain to source current even at zero gate potential, and a negative voltage is required to deplete the channel to switch off the device. Hence, the HEMTs are called depletion-mode devices contrary to enhancement mode transistors, where the gate voltage above zero volts is required to switch on the device. Since the applied gate voltage modulates the 2DEG in AlGaN/GaN HEMT, therefore the dependence of the sheet carrier concentration in the 2DEG region on applied gate voltage can be given as by modifying the Eq. (1.23) to the following expression [Balaz, 2011]:

$$n_s\,(x,d) = \frac{\sigma_b\,(x)}{q} - \left(\frac{\varepsilon_0\varepsilon(x)}{dq^2}\right)\left[(q\emptyset_b(x) - V_G) + \Delta(x) - \Delta E_C(x)\right] \tag{1.26}$$

where ϕ_b is the Schottky barrier height of the gate, Δ is the penetration of the conduction energy band into the Fermi energy level ε is the relative permittivity of the barrier layer, and V_G is the gate voltage.

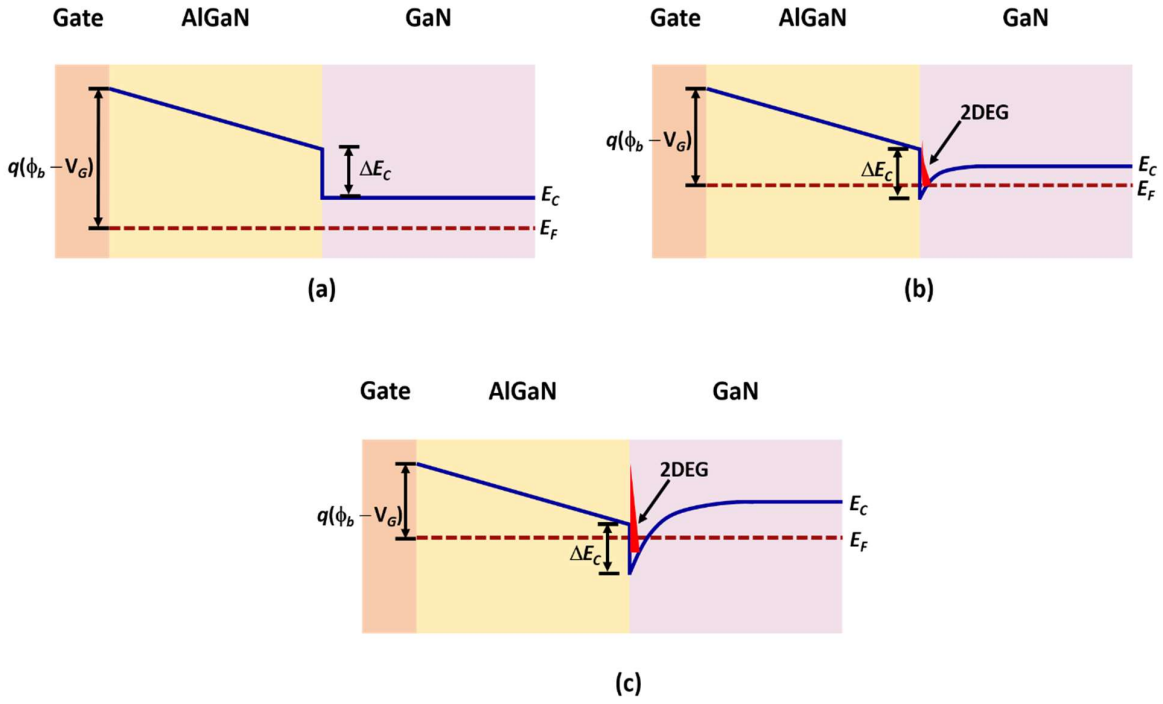

Figure 1.9: Energy band diagram of the AlGaN/GaN HEMT with 2DEG under different operating conditions: (a) cut-off (V_{GS}<V_T) (b) linear (V_D<(V_{GS}-V_T)) (c) saturation (V_D>(V_{GS}-V_T)) [Balaz, 2011]

Figure 1.9 illustrates the energy band diagram of the AlGaN/GaN HEMT with electron density at 2DEG at different gate voltages. It shows the operation of the HEMT under different operating regions, cut-off, linear, and saturation. In the saturation region, the 2DEG possesses high electron density. The electron density in the linear region is small compared to the saturation region and continuously decreases while approaching the threshold voltage (V_T). When the gate voltage is lower than V_T, ideally, there are no free electrons in the 2DEG to make the conduction, and the channel is fully depleted. The device in this condition is said to be under the cut-off region.

Generally, HEMTs are biased in common source configuration where the gate terminal is a controlling input terminal, the drain terminal is an output, and the source terminal is common to them. The controlling input gate has the capability to turn the HEMT on and off. Since AlGaN/GaN HEMTs are depletion mode devices; thus, a negative gate voltage requires to deplete the 2DEG channel. This negative gate voltage makes the channel highly resistive so that there is no drain to source current flow through the channel. In this situation, the device is under cut-off mode or said to be in pinch-off condition. Apart from Eq. (1.26), a relation between the number of charge carriers and applied gate voltage can be given as [Liddle, 2008]:

$$n_s = \frac{\varepsilon_{AlGaN}}{q(d_{AlGaN} + \Delta d)}(V_{GS} - V_T) \tag{1.27}$$

where Δd is the effective thickness of 2DEG from the AlGaN/GaN heterointerface, and V_{GS} is the gate to source voltage. When the gate to source voltage or gate voltage, V_{GS} is equal to threshold voltage V_T, the term (V_{GS}-V_T) is zero in the Eq. (1.27), and hence n_s goes to zero, and the device is said to be turned off. When V_{GS} = 0 V, the 2DEG possesses enough sheet carrier concentration,

sufficient for the conduction of drain current in the device. For the device operation condition, $V_{DS} < (V_{GS}-V_T)$, the device works in the linear region in which the charge carrier velocity in the 2DEG is proportional to the applied electric field. In this condition, the drain to source current (I_{DS}) can be given as:

$$I_{DS} = qn_s v_{eff} W_G \tag{1.28}$$

where W_G is the width of the gate, and v_{eff} is the effective carrier velocity of the charge carriers, i.e., electrons in the 2DEG. By utilizing the condition of the linear region, the relationship between electron velocity and applied electric field can be given as:

$$v = \mu_n E \tag{1.29}$$

where μ_n is the mobility of the electron in the 2DEG, and E is the applied electric field. From Eq. (1.29), it can be said that under the condition of the low electric field of $V_{DS} < V_{GS}-V_T$, the I_{DS} increases linearly with the electric field, and the device is said to be in the linear region. Using the above equations and the conditions for the linear region, the I_{DS} can also be expressed as:

$$I_{DS} = \frac{\varepsilon_{AlGaN} v_{eff} W_G}{2(d_{AlGaN} + \Delta d)} V_{DS}(2(V_{GS} - V_T) - V_{DS}) \tag{1.30}$$

At the high electric field, $V_{DS} > V_{GS} - V_T$, the velocity of electrons starts saturating and becomes independent from the applied electric field. At this time, the AlGaN/GaN HEMT moves into the saturation region where any further increment in the V_{DS} does not increase the I_{DS}. For the condition of saturation, the drain current, I_{DS} can be given as:

$$I_{DS} = \frac{\varepsilon_{AlGaN} v_{sat} W_G}{(d_{AlGaN} + \Delta d)} (V_{GS} - V_T) \tag{1.31}$$

where v_{sat} is the electron velocity in the saturation region, the Eq. (1.31) suggests that the gate width variation also affects the I_{DS} directly. Thus, the above set of equations express the working of AlGaN/GaN HEMT in different regions of operation.

1.3.4 Surface Traps

The traps are defined as energy states in the semiconductor energy band-gap, are situated at the surface of the device, as shown in Figure 1.8. These traps cause surface impurities, the formation of dangling bonds, and other surface defects. Their origin depends on several factors, such as threading dislocation, densities, defects in the crystal, and the existence of impurities. The surface traps can be either empty or occupied by electrons that significantly impact the charge conduction of the device. Traps that are closer to the conduction energy band are termed as acceptor-like traps. These traps are negatively charged during the occupancy of electrons and neutral when empty. Although, the traps which are closer to the valency energy band are known as donor-like traps. These traps are neutral under-occupied condition and positively charged when empty. These traps play a crucial role in the HEMT operation and its performance, as they can be the 2DEG source having positive charges, which can reduce polarization induced charges on the AlGaN surface. In AlGaN/GaN HEMTs, the surface traps also depend upon the thickness of the AlGaN barrier layer. The surface traps for the thin barrier layer of AlGaN are below the Fermi level, and all the surface states are neutral as they are fully occupied. As the thickness of the AlGaN barrier layer increases, the Fermi level starts moving towards the deep donor level, and hence electrons get sufficient energy to leave these traps to form 2DEG at the heterointerface of AlGaN/GaN HEMT, and the empty surface traps are being positively charged. Experimentally, the surface donor states have generally found at 1.65 eV and 1.42 eV below the conduction band in MBE and MOCVD structures, respectively, for the 2DEG development [Ibbetson *et al.*, 2000; Smorchkova *et al.*, 1999].

1.3.5 Self-Heating Effect

The advantage of the AlGaN/GaN-based HEMT is that they possess high electron density and wide bandgap, making it a suitable candidate for high power applications. However, in the high-power operation, the high electric field and the high current flow in the material generate a large amount of heat known as self-heating of the device. Because of the self-heating phenomenon, the lattice temperature rises. The increment of lattice temperature alters the temperature-dependent properties of the material, such as mobility and bandgap, which degrades the performance of the device. The performance of the device during high power applications mostly relies on the substrate choice and its thermal conductivity. The thermal conductivity of the substrate material suggests the amount of heat that can be dissipated by it. The research has been taken place for the analysis of different substrates like Si, SiC, and sapphire by electrothermal Monte-Carlo process [Sadi *et al.*, 2006], and it was observed that SiC delivers the maximum current with minimum temperature increment, which attributes the most suitable candidate for high-power applications.

1.4 HEAVY METAL ION SENSORS

The heavy metal ions sensors come under the category of chemical sensors. These sensors transform the information related to specific heavy metal ions into a useful analytical signal, which can be utilized for further signal processing. The heavy metal ions sensor comprises three basic building blocks: receptor, transducer, and signal processing unit, as shown in Figure 1.10.

(1) *Receptor:* A receptor is also called as recognizing or functionalizing element. It is a thin layer capable of making interaction with specific heavy metal ions. It can also improve the selectivity towards a particular heavy metal ion or a group of heavy metal ions. In the process of identification of particular heavy metal ions at the receptor/heavy metal ion interface, different receptors perform different reactions with heavy metal ions such as ion exchange, oxidation, reduction, redox, adsorption, liquid-solid or liquid-liquid interaction as shown in Figure 1.10. In most heavy metal ion sensing applications, the functionalizing element interacts with heavy metal so that the transducer gets enough information to generate the specific signal.

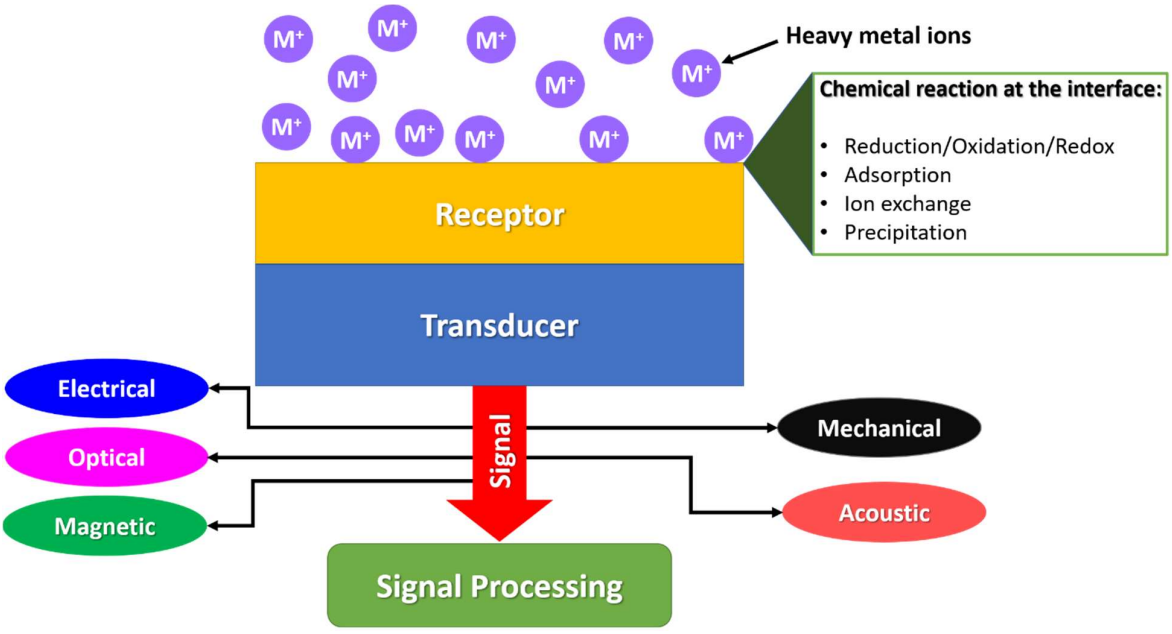

Figure 1.10: Generalized block diagram of the heavy metal ion sensor

(2) *Transducer:* A transducer in the heavy metal ion sensor converts the received information in the form of charges or heat into the desired signal like electrical, optical, mechanical, magnetic, and acoustic. Nowadays, the signal generated from the transducer is utilized for signal processing as well as a data storage perspective; hence, the electrical transducer is generally employed for the heavy metal ion sensing application, which can generate the signal in the form of current, voltage, and resistance.

(3) *Signal Processing:* The signal processing system is an instrumentation or sensing system utilized to analyze, store, and compare the received data. It can also represent the electrical circuits or electronic systems manages, which can process the received signal and perform the operations such as analog to digital conversion, amplification of the signal, and many more.

1.4.1 Importance of Heavy Metal Ion Sensors

The significance of clean and safe water has become an essential requirement for humans, and for maintaining the ecological balance as the fundamental necessity for every living organism is water. In the present scenario, a serious environmental challenge is coming because of the water pollution caused by agricultural and industrial waste, and hence, the insufficiency of clean water is continuously increasing. In general, water pollutants are broadly categorized as organic and inorganic water pollutants [Carolin *et al.*, 2017]. There are various physical, chemical, and biological processes being employed for the treatment of organic water pollutants. However, these approaches are not appropriate for the treatment of inorganic pollutants, such as heavy metals ions.

The heavy metal ions come from the micropollutants group, affecting many environmental components, including aquatic and earthly [Bansod *et al.*, 2017]. Heavy metals can be defined as natural elements having higher density and toxicity even at trace level concentration. The properties of heavy metals such as solubility, redox behavior, and formation of complexes, do not let to decompose them. Thus, once the heavy metals appear in the ecosystem, they can exist continuously for a long time for decades or centuries as these are inorganic pollutants [Gumpu *et al.*, 2015]. This non-biodegradable heavy metal waste is highly toxic and harmful to humans and other environmental systems and can produce severe diseases related to reproductive immune, gastrointestinal, and nervous systems [Gumpu *et al.*, 2015].

In the past few years, heavy metals in the water have become a serious concern. Industries such as pesticides, paper, metal plating, fertilizer, and mining operations release the heavy metal waste into the surroundings water sources such as a river, pond, or ground without proper treatment. The improper treatment of heavy metals generates the threat of vanishing the aquatic life, low oxygen levels in the water. While the heavy metals get released into the water resources, they transformed into hydrated ions. These hydrated ions are more toxic than the metal atoms, and its compounds can disturb the enzymatic process as well as cause the diseases as mentioned above much faster than metals and its compounds [Carolin *et al.*, 2017]. Hence the removal of heavy metals, its compounds, and its ions are essential for the ecosystem.

Amongst several heavy metal ions, arsenic (As), cadmium (Cd), chromium (Cr), lead (Pb), nickel (Ni), mercury (Hg), and zinc (Zn) are considered as highly toxic. These *Environmental health hazards* are in the top 10 rankings of the list issued by the *Agency for Toxic Substances and Disease Registry Priority List of Hazardous Substances* [Gumpu *et al.*, 2015]. The other part of the coin also explains that heavy metals are also required for the living organisms in minimal quantities to maintain metabolism, but the higher intake of these metals leads to carcinogen effects as well as fatal toxicity. Considering the harmful behaviors of heavy metal ions, various international agencies such as the World Health Organization (WHO) [WHO, 2011], International Agency for Research on Cancer (IARC), Centre for Disease Control (CDC), Environmental Protection Agency (EPA), Bureau of Indian Standards (BIS) have continuous monitoring on the concentration of metals in the water on priority basis [Gumpu *et al.*, 2015]. Moreover, the WHO, EPA, and BIS

have set the standard limits for different heavy metals, shown in Table-1.4, under which the concentration of these heavy metals ion in water is not harmful. Thus, the detection of these heavy metal ions in the water is vital to protect the environment.

Table 1.4: Standard guideline values for the maximum permissible limit of heavy metals ions in drinking water recommended by the WHO, EPA, and BIS [Aragay *et al.*, 2011; CWC, 2019; WHO, 2011].

Heavy metal ions	Standard guideline values (in ppm)		
	WHO	EPA	BIS
As^{3+}	0.01	0.01	0.01
Cd^{2+}	0.003	0.005	0.003
Cr^{3+}	0.05	0.1	0.05
Cu^{2+}	2	1.3	0.05
Pb^{2+}	0.01	0.015	0.01
Ni^{2+}	0.07	0.04	0.02
Hg^{2+}	0.001	0.002	0.001
Zn^{2+}	3	5	5

1.4.2 Heavy Metal Ions and Their Health Effects

As explained in the previous section, the toxic behavior of heavy metals like As, Cd, Cr, Cu, Ni, Pb, Hg, Zn, and so on generates a harmful health impact to the ecosystem. The ionic forms of these heavy metals such as As^{3+}, Cd^{2+}, Cr^{3+}, Cu^{2+}, Pb^{2+}, Hg^{2+}, and Zn^{2+} procedure toxic compounds the biological system, are vital to separate. Thus, it is necessary to know the behavior of these toxic heavy metal ions and their effect on health. Hence, the detailed description of the most common heavy metals and their potential health impacts is given as:

(a) Arsenic

Arsenic (As) is considered one of the most toxic and carcinogenic heavy metals. The global resources of arsenic, which can provide direct exposure to humans and other species, are fertilizers, pesticides, and untreated waste discharge. The arsenic contamination in water can affect peripheral and central nervous systems (PNS and CNS) and cause cardiovascular, hemopoietic, dermatologic, gastrointestinal, pulmonary, genitourinary diseases, and skin cancer [Gumpu *et al.*, 2015]. By observing the health impact of As ions on human health, the WHO set the standard limit for As ions, i.e., 10 ppb [WHO, 2008]. The concentration above this limit may severely harm human beings.

(b) Cadmium

Cadmium is generally found as natural deposits, also one of the most toxic heavy metals acquired in industrial waste. The primary industrial sources of cadmium are electroplating, cadmium-nickel batteries, synthetic rubber, phosphate fertilizers, stabilizers, engraving, and photographic process [Gumpu *et al.*, 2015]. At higher concentrations, there are severe harmful health effects caused by cadmium ions. The high concentration of cadmium ions in the river caused *Itai-Itai* disease, in which the softening of the bones, fractures, and skeletal deformation happens to human beings [Carolin *et al.*, 2017]. Furthermore, the health effects such as anemia, weight loss, hepatic toxicity, fatigue, atherosclerosis, lymphocytosis, lung cancer, and various diseases can harm the kidney, respiratory system, and liver [Carolin *et al.*, 2017; Gumpu *et al.*, 2015]. By considering the toxic behavior of cadmium, the WHO sets a permissible limit of cadmium ions in drinking water is 3 ppb (parts per billion), below which it does not harm human beings [WHO, 2011]. Hence, it is desirable to detect and remove the cadmium below the standard limits set by WHO. Further, the detailed description related to Cd^{2+} ion toxicity also is explained in chapter 5.

(c) Chromium

The Chromium comes in the seventh position in terms of availability in the earth. The most common industrial resources for chromium ions in water are leather, textile, and electroplating industries, which discharges their waste in the Cr (III) and Cr (VI) form. These two forms of Chromium are also employed in various industrial applications such as chrome polishing, steel production, glass, and electroplating industries. The exposure of chromium in water also makes a significant impact on human health by pulmonary congestion, liver and kidney damage, vomiting, ulcer, and skin inflammation [Carolin *et al.*, 2017]. By considering these health effects due to the chromium, it must be removed from the water or requires to modulate it so that the concentration of Chromium ions comes under the WHO permissible limits for drinking water, i.e., 50 ppb [Gumpu *et al.*, 2015] before discharging into the environment.

(d)Copper

Copper (Cu) is usually a very toxic metal at high concentrations, although Cu is an essential element required for living beings because of its active participation in enzyme synthesis and tissue and bone growth [Ding *et al.*, 2014]. There are three different forms in which copper is generally found; these are metallic copper (Cu^0), cuprous ion (Cu^+), and cupric ion (Cu^{2+}). Among them, the Cu^{2+} is more toxic than the other two forms. The industries which majorly extrude the copper wastes are electroplating, steel and mining industries, chemical manufacturing units, paints, and fertilizers [Carolin *et al.*, 2017]. There are numerous health effects on human health due to excessive copper ions in the water, such as hair loss, anemia, kidney damage, and headache [Tang *et al.*, 2014]. Due to these health impacts, the maximum permissible limit in drinking water set by WHO is 2 ppm [WHO, 2008]. Therefore, proper treatment of copper contaminated water is required to make the water reusable.

(e)Lead

Lead (Pb) is a very harmful metal which can cause several diseases to humans once it goes into the body. The effects of lead toxicity are more severe to children than adults. Lead is generally exposed in the water because of Lead-acid battery. The electrical, explosive, cosmetics, steel, paint, and electroplating industries are the primary resources that release lead and its compounds to the water [Nigam *et al.*, 2019b]. Although a minimal quantity of Pb is required to the human body as it helps in cell replication and DNA and protein synthesis, however, the higher concentration of lead can cause mental retardation, kidney and nervous system damage, illness, reduction in sensations, sleeping difficulties, abdomen pain, and cancer to the human body [Carolin *et al.*, 2017]. The toxicity of lead is more dangerous to children as it can cause severe diseases such as loss of developmental skills, reduction in IQ level, kidney damage, hearing loss, behavioral and attentional problems, slow body growth, and obstruct the development of nerves and brain. It also affects the plants and animals significantly. Therefore, the detection of lead in the water and the removal of its concentration below the WHO standard limit is highly required. Because of toxicological threats and effects on humans, the maximum permissible limit set by the WHO for the Pb ions [WHO, 2008] for drinking water is 10 ppb in their guidelines.

(f) Nickel

Nickel is a kind of heavy metal found in wastewater used in battery manufacturing units, silver refineries, production of stainless steel, printing, and electroplating industries. Additionally, it is also employed in different applications such as coins, catalysis, batteries, wires, jewelry, and machinery parts. In general, food is a dominant source of Ni exposure, whereas water minorly contributes to Ni intake. The excessive concentration of Ni is generally found in the groundwater and surface water near the industries mentioned above. The intake of Ni above the prescribed limit of WHO can cause skin eruption, diarrhea, dry cough, chest pain, nausea, pulmonary fibrosis, and also creates breathing problem [Carolin *et al.*, 2017; Yang *et al.*, 2009]. In order to overcome the possible health-related issues caused by Ni exposure in water, the WHO set its standard guideline value, i.e., 70 ppb [WHO, 2011], and hence the detection of Ni at lower concentration is required for its excessive content from the water.

(g)Mercury

Mercury (Hg) grabs the attention due to its highly toxic nature, and the case occurred in Japan [Kalimuthu *et al.*, 2009]. Mercury is the most toxic heavy metal in the water, which can exist in distinct forms such as Hg^0 (elemental mercury), mercurous (Hg_2^{2+}), and mercuric (Hg^{2+}) ions [Kumari and Chauhan, 2014]. The mercury can easily accumulate in aquatic systems. It can appear in the environment by different activities like coal combustion, oil refinement in refineries, volcanic emissions, incineration of municipal solid waste and by various industries, e.g., paper, plastic industries and can cause many disorders related to the brain, digestive system, respiratory system, kidney, eyes, lungs, and skin and diseases like Minamata, hypotonia, acrodynia, and hypertension [Carolin *et al.*, 2017; Gumpu *et al.*, 2015]. In order to protect the human from these diseases and disorders caused by mercury exposure, Minamata convention is adopted and regulated in 2013[Wu *et al.*, 2016a]. As per this convention, the products which have mercury and associated compounds must follow strict emission standards. By recognizing the health effect of mercury, the WHO also set its limit to 1 ppb in drinking water [WHO, 2008]. Moreover, the details related to mercury and its impact on human health are described in chapter 7.

(h)Zinc

Zinc is a heavy metal that supports the physiological operations and biochemical control processes of the tissues [Jellouli Ennigrou *et al.*, 2014]. Zinc can also be utilized as a protective layer for other metals and includes in galvanization processes. There are various industrial resources for Zn release in the environment: paper and pulp, electroplating industries, and steel manufacturing units. A small amount of Zn is required for metabolic activities. However, at higher Zn concentration, several health issues such as anemia, fever, vomiting, body pain, skin inflammation can affect the human body [Carolin *et al.*, 2017; Gumpu *et al.*, 2015]. The effects mentioned above, together with the need for an effective treatment for removing zinc from the wastewater. Hence, the WHO sets its standard limit as 3 ppm for drinking water [WHO, 2008].

The discussion related to heavy metals and their adverse effects on human health and the environment suggests a requirement of sensitive and selective determination of heavy metal ions below the WHO permissible limits. Thus, various approaches have been developed to detect these heavy metal ions in water, as explained in the next section.

1.4.3 Classification of Heavy Metal Ions Sensors

In order to detect heavy metal ions at trace and sub-trace levels, various methods have been developed for the advancement of heavy metal ion sensors. Figure 1.11 shows the broad classification of different types of heavy metal ion sensors, such as electrochemical, colorimetric, biological, and semiconductor-based. These sensors have been classified on the basis of the used approaches, materials, and functionalizing elements. In addition, there are several spectroscopic techniques such as atomic absorption spectroscopy (AAS), inductively coupled plasma mass spectroscopy (ICP-MS), and inductively coupled plasma-optical emission spectrometry (ICP-OES) are utilized for the detection of heavy metals ions in the aqueous solutions. These techniques are suitable for the simultaneous detection of heavy metal ions over a long range of concentrations from the femtomolar to the millimolar range. Though, these methodologies are very costly and involve trained staff for handling its complex equipment. Moreover, these methods require a sophisticated analytic process for sample preparation as well as have the high-risk during sample handling, changing, and storing processes [Bansod *et al.*, 2017]. Thus, the sensors mentioned above, as well as in Figure 1.11, are essential to fulfill the requirement of heavy metal ion detection in aqueous solutions. The comprehensive description of these heavy metal sensors is explained as follows:

(a) Electrochemical heavy metal ion sensors

Electrochemical heavy metal ion sensors are the type of chemical sensors in which electrochemical techniques were employed for heavy metal ions detection in an aqueous solution. The classification of these sensors depends on the various electrical signals such as voltage,

current, impedance, charge, and electrochemiluminescence, which were produced in the solution due to the heavy metal ions. Based on these electrical signals, the electrochemical process that can be utilized for heavy metal ion sensing can be categorized as Amperometric, Voltammetric, impedance measurement, electro-chemiluminescent based ion sensors [Bansod *et al.*, 2017]. Such methods utilize either current or voltage as a controlling parameter to analyze the change in another one. In the electrochemical sensor, two or three-electrode system were used for heavy metal ion detection. These electrodes are a working electrode, a counter electrode, and a reference electrode. On the working electrode, the detection of heavy metal ions is performed by functionalizing the electrode for specific metal or group of metals. The counter or auxiliary electrode is used to perform the other rection and is required for the current flow. A fixed voltage or current is applied between the electrodes, and correspondingly, other variables, either current or voltage, are measured in a two-electrode electrochemical ion sensor. The working and counter electrode makes a circuit over which the voltage or current can be applied or measured in the three-electrode system. In this system, the potential at the working electrode can also be measured against a reference having stable and known potential.

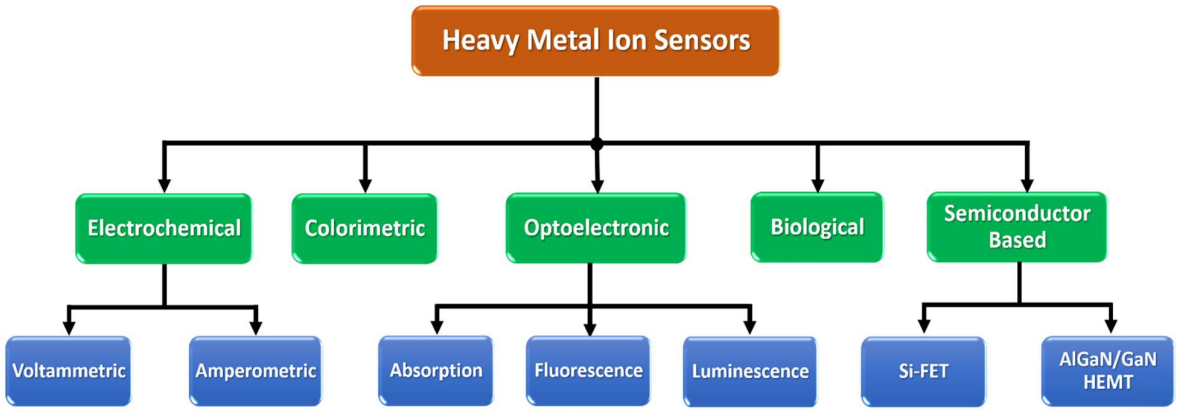

Figure 1.11: Classification of heavy metal ion sensors

(1) *Amperometry based heavy metal ion sensors:* Amperometry is the process that belongs to electrochemical methods in which the current is measured at a fixed applied potential at the working electrode. Herein the fixed potential is applied between the working and reference electrode in the heavy metal ion solution. The change in the measured current suggests the reaction mechanism happening at the working electrode, which indicates the concentration of heavy metal ions in the solution. The response in the form of current is measured with respect to time.

(2) *Voltammetry based heavy metal ion sensors:* Voltammetric techniques are extensively utilized in heavy metal ion detection because of its high accuracy and sensitivity. It is used by measuring current at the various potential in an I-V contrary to the fixed potential in the amperometric analysis.

(b)Colorimetry based heavy metal ion sensors

Colorimetry is another sensing technique that is widely employed in heavy metal ion sensing applications. It detects the change in color due to a chemical reaction between the heavy metal ions and the functionalizing element. The advantage of utilizing colorimetry based heavy metal ion sensors is the simultaneous detection of different heavy metal ions in an array [Lin *et al.*, 2018]. Nowadays, the colloidal nanoparticles (NPs) of different metal ions such as gold and silver are generally utilized for colorimetric detection. The binding of heavy metal ions to the surface of nanoparticles leads to aggregation, which results in the color change. Surface Plasmon Resonance (SPR) is an exclusive phenomenon showed by metal NPs which happens when coherent oscillations of the electrons in the conduction band resonate with the electromagnetic

radiation's frequency [Priyadarshini and Pradhan, 2017]. Since most of the reactions for colorimetry analysis are irreversible, the colorimetry-based heavy metal ion sensors are single-time usable for the analysis of heavy metal ion detection. Hence these sensors are not suitable for continuous and reliable heavy metal ion sensing.

(c) Optical sensors for heavy metal ion detection

Optical heavy metal ion sensors are the type of sensor which detects optical changes in the input due to the heavy metal ion and recognizing element interaction. These changes determine the concentration of the heavy metal ions present in the water. Optical heavy metal ion sensors exhibit several advantages such as they require small instrumentation, insensitive towards electromagnetic interference, and a simple structure. Depending upon the mechanism, these sensors are classified as Absorption based, Fluorescence-based, and luminescence-based ion sensors [Odobašić *et al.*, 2019].

(1) *Absorption-based heavy metal ion sensors* determine the concentrations of various heavy metal ions on the basis of absorbance of heavy metal ions at a particular wavelength of light, incident on the sample. This light travels from the light source to the sample and from the sample to the detector via optical fiber.

(2) *Fluorescence-based heavy metal ion sensors* determine the target heavy metal ions in the water by observing the variation in the emitted electromagnetic radiation frequency. The frequency change is measured by the absorption of radiation and the presence of the excited state of the target heavy metal ions.

(3) *Luminescence-based heavy metal ion sensors* are the type of sensors whose working principle is based on chemiluminescence in which the emission of light happens due to the chemical reaction between heavy metal ions and recognizing elements. These sensors are easy to use and show results as visible in terms of luminescence.

(d)Biosensors for heavy metal ion detection

Biosensors provide an easy, fast, and reliable way to detect different heavy metal ions in the water. These are small-sized devices that can perform in-situ applications, advantageous over long-term and expensive laboratory experiments. Biosensors detect the presence and specific concentrations of heavy metal ions in water and suggest their biological effects like toxicity. In general, biosensors utilize biological elements such as DNA (Deoxyribonucleic acid) and enzymes for the detection of heavy metal ions[Gumpu *et al.*, 2015].

(e)Semiconductor based heavy metal ion sensors

In general, a semiconductor-based heavy metal ion sensor utilized the field-effect transistor for sensing applications. A field-effect transistor (FET) measures the flow of current between the source and drain terminal, controlled by an external applied electric field applied at the gate terminal. Ion-selective field-effect transistors (ISFETs) are a special type of sensors that utilizes the electronic devices in the combination of electrochemistry for the detection of heavy metal ions. Here, the surface of the gate terminal is functionalized for the detection of target molecules. Based on the reaction performed between the heavy metal ions and the functionalizing element, the electric field at the gate terminal changes, which in turn modulates the charges in the channel region and hence, the drain to source current of the ISFET changes. ISFET sensors are currently utilizing in numerous applications for chemical and environmental sensing applications because of their electrical and chemical properties. Modern ISFET sensors miniaturized the complete sensor that generates the integration possibility into the electronic world [Asadnia *et al.*, 2016]. These devices are compact, which makes it perfect for portable sensing applications. In the early stages, the ISFETs have developed a substantial interest in the research, which was observed in the number of publications [Bergveld, 2003]. The Si-FETs have become mature devices in terms of ISFETs, which are being utilized not only in heavy metal ion

sensing applications but for biological and other environmental applications also. Besides, the Si-ISFETs have also provided benefits in terms of cost-effective mass production of heavy metal ion sensors. However, the ISFETs lag in the long-term chemical stability in the aqueous solutions and require proper insulation [Schöning *et al.*, 1996].

Nowadays, the advancement of the ISFETs occurs in the form of utilizing new devices such as AlGaN/GaN HEMT for next-generation sensing applications. These HEMT based heavy metal ion sensors provide the sensitive and rapid determination of ions and superior stability due to its unique properties, as discussed in the previous sections. A detailed description of the AlGaN/GaN HEMT based sensor is provided in upcoming sections.

1.4.4 Desirable Characteristics of Heavy Metal Ion Sensors

The performance of heavy metal ion sensors is generally described and compared based on various parameters like sensitivity, selectivity, response time, dynamic range, linearity, the limit of detection, and lifetime [Grundler, 2006]. These parameters also define the specialty and applicability of the sensor in different applications. The following parameters are utilized for characterization and evaluation of the performance of the heavy metal ion sensor:

(a) Sensitivity

Sensitivity is an important parameter of a heavy metal ion sensor, which can be defined as the relative change in the measured signal per unit concentration of the heavy metal ions. In other words, it can also be described as the slope of a calibration curve. A sensor should possess high sensitivity for the detection of heavy metal ions.

(b) Limit of Detection

The *limit of detection (LoD)* is the lowest concentration of the heavy metal ions in the solution detected by the sensor using a particular analytical method. The limit of detection is also defined by the *International Union of Pure and Applied Chemistry (IUPAC)* in 1975, "the limit of detection, expressed as a concentration, is derived from the smallest measure that can be detected with reasonable certainty for a given analytical procedure"[Long and Winefordner, 1983]. In order to effectively measure or to perform reliable detection of heavy metal ions, there are different approaches utilized for the determination of limit of detection.

(1) *Based on visual analysis:* The limit of detection is examined by evaluating samples with known analyte concentrations and observation of the minimum concentration level at which the reliable detection of the analyte can be possible[Shrivastava and Gupta, 2011].

(2) *Based on the Signal-to-Noise ratio:* The limit of detection can also determine by the signal-to-noise ratio analysis, achieved by comparison of response measured from samples of known low concentrations of analyte with the response observed from the blank sample. In general, the acceptable value of the signal-to-noise ratio is 3:1 for the estimation of the LoD [Jung *et al.*, 2009].

(3) *Based on the Standard Deviation of the Response and the Sensitivity:* The calculation of the limit of detection can also be performed using the standard deviation of the response and the slope of the calibration line or sensitivity of the response. The following expression gives the relation between the sensitivity and limit of detection of the sensor [Magnusson and Örnemark, 2014; Shrivastava and Gupta, 2011].

$$LoD = \frac{3\sigma}{m} \tag{1.32}$$

Here σ is the standard deviation of the response, and the m is termed as the sensitivity of the sensor. In this work, the limit of detection was calculated by utilizing the sensitivity and standard deviation of the developed sensors for heavy metal ion detection, as described in Eq. (1.32).

(c) Selectivity

Selectivity or specificity describes the ability of the sensor to detect specific heavy metal ion or a specific group of ions in the presence of other heavy metal ions in the solution. Thus, the selectivity of a developed sensor should be high, i.e., the interference of other heavy metal ions on the characteristics should be minimum. The term selectivity coefficient generally determines the selectivity of an ion sensor. Researchers use different methods, such as the separate solution method and the mixed solution method. There are two variants used in the mixed solution methods: fixed analyte method and fixed interference method. In the fixed analyte approach, the analyte (here the metal ions which is to be detected) concentration has been set at a particular value, and the concentration of the interfering metal ion has been varied. In contrast, in the fixed interference method, the concentration of interferent metal has been fixed at particular concertation, and the analyte concentration is varied [Maccà and Wang, 1995]. The change in the response of the sensor describes the selectivity of the sensor.

(d) Response and Recovery Time

The response time of a heavy metal ion sensor is defined as the time required to change the response of the sensor from 10% to 90% after making the change in the concertation [Chang *et al.*, 2011]. The response time is a crucial parameter that shows the effectiveness of the sensor in terms of fast detection. The recovery time is the time taken by the sensor to reach its baseline (response at the blank solution) from 10% to 90% after applying the solution. The response and recovery time should be as low as possible for a highly efficient heavy metal ion sensor.

(e) Dynamic and Linear Range

Dynamic range specifies the range concentration between the limit of detection and concentration, where the sensor starts saturating. It describes the working range of the sensor [Grundler, 2006]. On the other hand, the linear range is the relative standard deviation of the measured calibration graph from a straight line. Generally, the linear range describes a definite range of heavy metal ion concentration [Grundler, 2006].

(f) Repeatability and Reproducibility

Repeatability and reproducibility are methods of determining the precision of an ion sensor. The repeatability of the sensor was observed by performing the sensing operation under the same operating conditions. In contrast, reproducibility is the agreement between the sensing responses observed under different operating conditions as well as on different samples.

1.4.5 AlGaN/GaN HEMT as Heavy Metal Ion Sensors

The III-N devices are widely employed in high power, high frequency, and optoelectronic applications. Specifically, the confinement of electrons at AlGaN/GaN heterojunction in the HEMT to form 2DEG due to spontaneous and piezoelectric polarization showed promising results for these applications. At the same time, the availability of dangling bonds at the surface of AlGaN/GaN HEMT, also called surface states, makes the device extremely sensitive to any changes at the surface. These surface-states significantly affect the device operation, as discussed previously in section 1.3.4. Although this problem is a disadvantage of AlGaN/GaN HEMT for the high power, high-frequency applications, simultaneously, this disadvantage has become a significant advantage while the AlGaN/GaN HEMTs have utilized in the chemical sensing as well as ion sensing applications and hence have received much attention since last decade [Cimalla *et al.*, 2011; Eickhoff *et al.*, 2001; Pearton *et al.*, 2004].

Because of the unique material properties of AlGaN/GaN HEMT, such as wide bandgap and strong bond strengths, it shows excellent chemical stability during wet etching processes [Cimalla *et al.*, 2011]. With the availability of highly sensitive surface because of surface traps and low noise owing to the wide bandgap characteristics [Cimalla *et al.*, 2011] and high sensitivity to changes of the surface charge, AlGaN/GaN HEMTs have become the most promising candidates for various sensing applications and have been utilized for detecting pH [Steinhoff *et al.*, 2003],

peptide [Rohrbaugh *et al.*, 2014], prostate-specific antigen [Wang *et al.*, 2007], DNA hybridization [Thapa *et al.*, 2012], glucose [Chai *et al.*, 2010] and heavy metal ions like mercury [Asadnia *et al.*, 2016; Chen *et al.*, 2008], lead, and cadmium with good sensitivity and fast response time by the surface modification at the gate region of the AlGaN/GaN HEMT.

In the AlGaN/GaN-based heavy metal ion sensors, the connection of the 2DEG channel is made from source, and drain terminals, modulated by the potential at the gate terminal. For sensing applications, the gate is exposed in the sensing environment, i.e., the reaction performed at the gate region varies the charges, and hence 2DEG modulates. The detection of heavy metal ions using this technique is easy, quick, and reliable. The observed sensing response can also be easily quantified, transmit, and stored contrary to the fluorescence sensing process where human inspection is highly required and difficult to precisely identify and store or transmit the sensing results [Ren *et al.*, 2011]. The only drawback of AlGaN/GaN HEMT sensors is the lack of selectivity towards specific heavy metal ions, which can be resolved by modification surface at the gate region by target heavy metal ion-specific functionalization.

1.4.6 Advantages of AlGaN/ GaN HEMT Based Sensors Over Other Methodologies

As discussed in section 1.4.3, there were many methods and sensors utilized to detect heavy metal ions in water. The spectroscopic techniques such as atomic absorption spectroscopy (AAS), inductively coupled plasma mass spectroscopy (ICP-MS), and inductively coupled plasma-optical emission spectrometry (ICP-OES) shows excellent detection of heavy metal ions in water from femtomolar to millimolar range. However, these are laboratory-based and very expensive approaches that require a specialist operator for operation. [Bansod *et al.*, 2017]. Since these techniques exhibit excellent performance under laboratory conditions, there is a requirement for small, portable, and fast sensors having the capability of wireless connectivity that has the capability for fast responses. In addition, the sensors should have high sensitivity and selectivity with a fast response time.

In order to make the small-sized, portable heavy metal ion sensor, the Electrochemical heavy metal ion sensor made the attraction because of their cost-effectiveness and simple structure; however, these sensors are difficult to use for frequent onsite determination of heavy metal ions. The colorimetry sensors are also small-sized sensors and useful for onsite determination of heavy metal ions by showing the color vision change. However, the main drawback of these sensors is that the reaction performed in this process is irreversible, so the repeatability of response is very hard. Furthermore, by visualizing the response of the sensor, it is challenging to determine the precise value of the concentration [Lin *et al.*, 2018]. These disadvantages limit the application of colorimetry sensors for widespread use in heavy metal ion sensing.

Optical heavy metal ion sensors exhibit several advantages such as they require small instrumentation, simple structure, and do not get affected with any electromagnetic interference. Hence, these sensors can be utilized for portable applications of heavy metal ions sensing. Though, as explained in the previous section, these sensors require continuous monitoring; hence, the presence of a person is required to monitor the sensing response every time [Ren *et al.*, 2011].

The semiconductor-based sensors can be fabricated by employing Si substrate, as the Si industries are well matured that can utilize the standard and optimized process along with novel nanotechnology methods to develop the advanced ion sensors. The sensors based on Si are still dominating in the semiconductor industries because of their cost-effective, reproducible, and controlled sensing response. However, the Si-based sensors are not appropriate for harsh environment operations such as high temperature, high pressure, and corrosive situations. Further, the Si can be easily affected and etched by some acids and bases, which can disturb the sensor and its characteristics. Additionally, Si-based devices also suffered from the drift and lack

of chemical stability in the solutions. Moreover, the enhancement type Si-ISFETs, which are used in the chemical, as well as biosensing applications, are normally-off. Thus, there is a requirement for the reference electrode to provide sufficient gate potential to the ISFET (above the threshold voltage) to flow the charge carriers through the channel. Although the depletion type Si-ISFETs can be used without a reference electrode, their fabrication requires heavy doping to make them normally-on. The heavy doping in the device can decrease the performance of the device. Thus, most Si-ISFETs are enhancement type devices, and the employment of the reference electrode as an essential component of the sensor increases the fragility and bulkiness of the sensor. In order to solve this problem, the fabrication of on-chip Ag/AgCl reference electrodes has been carried out; nevertheless, their fabrication process is very complex, and solution leakage of the electrode persists a severe problem, which ultimately reduces the accuracy lifetime of the sensor. Thus, there is a requirement of the sensors having an inert chemical surface along with the capability of working in harsh environmental conditions [Ren *et al.*, 2011].

Contrary to Si, GaN is a chemically inert material, cannot be etched by any acid or base. Thus, the III-N materials group and the devices provide an alternative solution to replace Si in the sensing applications. Moreover, the high chemical resistance, capability of working at high temperatures, high power applications flawlessly, and ease of integration with existing GaN-based technologies make these sensors an ideal candidate in heavy metal ion sensing applications. Besides this, the conventional AlGaN/GaN HEMTs are normally-on devices, i.e., having negative threshold potential, which means a negative gate voltage is required to turn off the device. Thus, these devices possess very high electron density at 2DEG channel without applying any gate voltage, and hence these device does not require any reference electrode for sensing application [Nigam *et al.*, 2019b]. Further, they also possess higher transconductance and excellent chemical stability.

It has been observed that the AlGaN/GaN HEMT devices have high sensitivity because of the availability of surface charges, which directly affect the 2DEG channel. Since there is high electron density at 2DEG due to quantum confinement and hence there is very small scattering compared to Si-ISFET devices, which significantly improves the sensing efficiency of the sensor. Therefore, the AlGaN/GaN HEMT based sensors are an excellent replacement to Si-ISFETs for next-generation sensing technologies for heavy metal ion detection.

In this thesis, these properties of AlGaN/GaN HEMT were utilized for heavy metal ion sensing applications, and the results suggest that there is no need for reference electrode for sensitive and selective determination of heavy metal ions.

1.5 MOTIVATION

GaN-based devices have made a special position in industrial applications by sustaining at high power and providing a maximum cut-off frequency. The III-N technology exploited the advantage of the high critical breakdown fields and benefited from high saturation velocity in GaN. According to a recently published report in "The Express-wire" on August 2019 with the headline "Gan Semiconductors Device Market 2019 Global Industry Company Profile, Brief Analysis by Regions, Market Size and Growth, Future Growth, Future Scope and Trends by Forecast 2023", in 2017, the GaN technology market was evaluated at US$ 711.44 million and is likely to reach at US$ 1.8428 billion by 2023 with compound annual growth rate (CAGR) of 17.1% between 2018 and 2023 [More, 2019]. The properties of III-N make them the most attractive material family for numerous applications, including but not limited to high power, high temperature, high-frequency applications including radar systems, military, and space applications. In recent years, substantial interests have also been developed in the field of optoelectronics and sensing applications such as ultraviolet (UV), blue light-emitting diodes (LEDs), and devices, light-sensitive devices, and next-generation light, ion, and gas sensors.

The continuously increasing demand for the power sector in the semiconductor industries and growing demand in consumer electronics, especially in LED-based displays and cumulative requirements of electric vehicles and photovoltaic inverters, are major application areas for the market of III-N semiconducting devices. The continuous growing demand for gaming consoles, smart devices such as smartphones, smart TVs, and laptops are also making III-N devices a potential candidate for semiconductor industries, as well as for consumer electronics. Besides this, the replacement of compact fluorescent light (CFL) lamps with LED bulbs in low power electrical applications offers many opportunities for GaN applications in the semiconductor industries. The compatibility of III-N devices in power and high-frequency applications make them the most eligible candidate for wireless electricity (WiTricity) like wireless charging, wireless switching applications for home appliances, and the development of electric and self-driving cars [More, 2019].

Initially, the production of GaN devices was costly. However, the continuous growth in the research and innovation and the competition between the leading industry players reducing the cost of the III-N technology. Furthermore, due to the growing production and high export rate of consumer electronics from China and Japan, East Asian countries are probably having the highest market share of GaN technology by 2023 [More, 2019]. Nowadays, China has the biggest electronic market for electric vehicles in the world. By observing these possibilities, Tesla Motors announced to begin its first manufacturing site in China in 2017 [More, 2019]. Correspondingly, India is showing commitment to sell only electric cars by 2030 under the new plans of the government to control pollution. Thus, India's biggest car manufacturing company, Maruti-Suzuki, has collaborated with Toyota to launch its first electric car in India [More, 2019]. These factors start the demand for III-N in India.

Besides this, an investment of 2.5% of the Gross Domestic Product (GDP) has been announced by the government of India for the healthcare sector [More, 2019]; this factor also opens the door for the III-N semiconductors and devices in the healthcare segment in India. Since human health is another serious issue that is started to be considered more sincerely worldwide, this paves the way for the researchers for the interdisciplinary work to develop fast, efficient, and smart devices for the health care sector. In the continuation of the research in the health care sector, the AlGaN/GaN HEMTs have shown the ability for the chemical and biochemical sensing applications comprising industrial processes, pharmaceutical, medical research, and water analysis applications. The HEMT is the right candidate, particularly for chemical and ion sensing due to its capability of being stable in harsh environments, low toxicity, high conductivity sensitivity to surface conditions, and functionality of ungated surfaces. These properties of AlGaN/GaN HEMT make a new pathway to develop the fast and miniaturized sensors for the ultimate use in the detection of toxic heavy metal ions such as cadmium (Cd), lead (Pb), and mercury (Hg).

1.6 RESEARCH OBJECTIVE

This research work is focused on the studies and development of AlGaN/GaN HEMT and their utilization for the sensing application to detect toxic heavy metal ions. As discussed earlier, III- N materials and a device like the AlGaN/GaN HEMT are most emerging candidates for the last three decades and have much potential in diverse applications such as high power, high frequency, and high-temperature applications. Still, the limits of the III-N material system and the devices are yet to be identified. In these regards, there are some objectives have set for this work, these are:

(1) Simulation of AlGaN/GaN HEMT and validation of observed electrical characteristics with experimental results. After validating electrical characteristics, the study of other parameters such as piezoelectric polarization, electron density, and tunneling probability will be carried out.

(2) To determine the impact of the self-heating effect on the electrical characteristics of the AlGaN/GaN HEMT.

(3) Fabrication of AlGaN/GaN HEMT on Si (111) wafer for the sensing application of heavy metal ions.

(4) Development of MPA-GSH functionalized Au-gated AlGaN/GaN HEMT for toxic Cd^{2+} ion detection. It can detect the Cd^{2+} ions below the WHO maximum permissible limit in water with rapid response and good selectivity.

(5) Detection of Pb^{2+} ions by functionalizing 2,3, di-mercapto, 1,3,4 thiadiazol (DMTD) at the gate terminal of AlGaN/GaN HEMT. The sensor should be highly sensitive and selective towards Pb^{2+} ions. The sensor is expected to provide the real-time determination of Pb^{2+} ions in the lake as well as tap water.

(6) Ultrasensitive and selective determination of Hg^{2+} ions using hydrothermally grown 2D-MoS_2 on AlGaN/GaN HEMT. The structural and electrical characterization of MoS_2 functionalized AlGaN/GaN HEMT should be performed before the sensing analysis. The sensing of Hg^{2+} ions using MoS_2 functionalized AlGaN/GaN HEMT is expected to provide high sensitivity, selectivity, excellent repeatability, along with rapid response in order to make it an excellent sensor for Hg^{2+} ions.

1.7 THESIS ORGANIZATION

In *chapter 2*, the simulation work has been carried out for AlGaN/GaN HEMT on the Sentaurus TCAD simulator tool, and corresponding the validation of the observed simulated electrical results will be performed with experimental results. Further, the effect of self-heating on the electrical characteristics of the AlGaN/GaN HEMT was also analyzed by simulation. Additionally, theoretical modeling for the surface analysis of AlGaN/GaN HEMT will also be explained for the heavy metal ion sensing.

In *chapter 3*, a brief description of the different techniques utilized for the fabrication and characterization of AlGaN/GaN HEMT will be illustrated.

In *chapter 4*, the process followed in the fabrication of AlGaN/GaN HEMT will be described. This process flow indicates step by step development of AlGaN/GaN HEMT, which will be further utilized for heavy metal ions sensing application. In addition, the electrical characteristics of the developed AlGaN/GaN HEMT will also be explained.

Chapter 5 illustrates the development of the Cd^{2+} ion sensor by functionalizing Au gated AlGaN/GaN HEMT by MPA and GSH and reveals the sensitive, selective, and rapid detection of cadmium ions using the developed sensor below the WHO standard maximum permissible limits.

Chapter 6 discuss the fabrication of the AlGaN/GaN HEMT sensor for Pb^{2+} ion detection. Here the gate region of AlGaN/GaN HEMT was functionalized by DMTD. Further, the analysis of the real water samples, such as lake and tape water also performed and verified by the standard techniques ICP-MS.

Chapter 7 reveals the detection of Hg^{2+} ions by the functionalization of hydrothermally grown MoS_2, a 2D material on the Au-gated AlGaN/GaN HEMT. The structural and electrical characterization of MoS_2 functionalized HEMT was carried out, and after that, the detection of Hg^{2+} ions using this sensor was performed, and results indicate the ultra-sensitive and selective determination of Hg^{2+} ions.

Chapter 8 draws the conclusion and corresponding future work that could be carried out for next-generation sensing applications.

…